High-Performance Shape-Memory-Polymer (SMP) Composites *via* Optimization of Multi-Dimensional Graphitic-Carbon Fillers and Development of Heat-Fire-and-Smoke Alarm-Devices Using SMP-Composites

Jeet Vishwakarma[1,2], Shubham Jaiswal[1,2], Chetna Dhand[1,2], Reuben J. Yeo[3], Hui Ru Tan[3], Rajeev Kumar[1,2], Pradip Kumar[1,2], Narendra Singh[1], Alka Mishra[1,2], Ajay Naik[1,2], Avanish K. Srivastava[1,2], Neeraj Dwivedi[1,2*]

[1]CSIR-Advanced Materials and Processes Research Institute, Bhopal- 462026, India

[2]Academy of Scientific and Innovative Research (AcSIR), Ghaziabad- 201002, India

[3]Institute of Materials Research and Engineering (IMRE), Agency for Science, Technology and Research (A*STAR), 2 Fusionopolis Way, Innovis #08-03, Singapore 138634, Republic of Singapore

Corresponding Author

[*] **Email:** neeraj.dwivedi@ampri.res.in (N. Dwivedi) **and** neerajdwivedi6@gmail.com

Abstract

Understanding how sp^2 carbons of different dimensionality engineer the shape memory polymer is crucial for fundamental science and developing next generation technologies. Further, with modernization, widespread adoption of rechargeable lithium-ion batteries, as well as hotter, drier weather attributed to climate change, have indirectly led to a globally increasing trend of fire-related accidents. To prevent such accidents from causing large-scale destruction and casualties, the rapid detection of a fire event is extremely important. In this work, we have developed mechanically robust shape-memory polyurethane (PU) composites containing graphitic-carbon fillers that exhibit good thermo-responsiveness. Reinforcement of the PU matrix by three types of graphitic-carbon fillers, namely 3D graphite, 2D multilayer graphene and 1D multiwall carbon nanotubes, yielded 36–47% and 20–29% faster shape-recovery in hot-water and hot-air environments, respectively, with minimum shape recovery time of 14 s in former and 106 s in latter environments, thermal conductivity enhancement of 15% to 55%, enhanced shape-recovery ratio (up to 100%), increased shape recovery stress by ~ 34–96%, lowered coefficient friction by 2–3 times, and improved wear resistance with respect to pristine PU. We found that a low concentration (~0.02–0.2 wt%) of all three types of fillers was adequate to enhance the thermal conductivity and shape recovery ratio while maintaining the composite's stretchability, whereas higher-filler concentrations (~1.0–2.0 wt%) were required to substantially increase the shape recovery speed and improve the tribological properties. Finally, PU-graphite composites were integrated into two embodiments of fire alarm device prototypes that we developed and were found to work efficiently and reliably under various simulated environments and field tests.

Keywords: Fire alarm device, actuators and sensors, shape memory polymers, graphitic carbons, thermo-responsive polymers, tribology

1. Introduction:

Shape memory polymers (SMPs) have attracted significant scientific and technological interest [1, 2], especially in the areas of industry automation, robotics [3-6] and artificial intelligence-based technologies [7-11]. The attractiveness of SMPs for such applications is attributed to their multi-stimuli-responsiveness [12-14], while at the same time being lightweight [15, 16], highly flexible [12, 17-19], and resistant to degradation even in extreme environments[20, 21]. Shape memory polyurethane (PU) is one such interesting SMP that contains both soft and hard segments in its network and possesses shape-morphing properties [22-25]. However, the thermal and electrical conduction properties, as well as the shape-switching response time of SMPs, including PU, remain poor [26-28].

Graphitic carbons (sp^2-rich) are present in various dimensionality such as 3D graphite, 2D graphene (or multilayer graphene), and 1D multiwall carbon nanotubes (CNTs) and display outstanding electrical and thermal properties [29]. Hence, many of these graphitic carbon materials have been used as fillers to tune the properties of shape memory materials including SMPs and shape memory alloys (SMAs). For example, a shape memory alloy nanocomposite of copper aluminium doped with NiTi-CNT was developed that demonstrated maximum elongation of 11.1% and shape recovery of up to 70% [30]. In the Cu-Al-Ni shape memory alloy, the Ni was replaced with 0.2% graphene reinforcement to make a Cu-Al-Graphene composite that displayed a better shape recovery cycle [31]. Macroscopic graphite particulates were also incorporated into shape memory alloys to develop composites with enhanced damping performance [32].

In particular for SMPs, 3D graphite (GT) [33], 2D MGR [34], and 1D CNTs [35] have all been proposed as suitable fillers for SMPs in separate research works. However, there is limited literature that demonstrates the simultaneous cross-comparison of 1D/2D/3D sp^2

carbons in controlling the mechanical, thermal, shape memory, and other functional properties of PU using a similar preparation method. Thus, a longstanding concern is the uncertainty in choosing the most suitable type of graphitic carbon filler for the reinforcement of SMPs, including PU, as well as the optimum concentration of filler for various applications. For example, when SMPs are to be used in moderate-to-high wear applications, they must have good wear durability and low friction under contact sliding environments[36]. Likewise, when SMPs are needed in smart devices where fast shape switching is required, suitable graphitic carbon filler type(s) and their optimum concentration are prerequisites to achieve fast shape recovery speed and improved thermal and electrical conduction without compromising the composite's mechanical performance. Thus, for graphitic carbon incorporated PU composites, it is crucial to optimize and enhance their shape memory and tribological properties and understand the underlying mechanisms of graphitic carbon reinforcement. Moreover, critical aspects of these fillers in regulating mechanical properties, such as strain of PU matrix, is not well understood so far. Furthermore, the application of these modified PU composites in the development of new smart devices must also be undertaken for technological advances, which is also one of the major objectives of this work as elaborated sub-sequentially.

We identify a critical application where the sensitive and stimuli-responsive shape memory behaviors of SMPs can be harnessed. With the modernization of technology and climate change, fire accidents have become more common, posing a severe threat to national infrastructure, the economy, human and animal life, and the environment when they grow out of control [37]. The increasing adoption of rechargeable lithium-ion batteries in modern devices has increased the occurrence of battery fires caused by overcharging or improper charging of these batteries. Prolonged and more frequent heatwaves have also increased the number of wildfire outbreaks across the globe, which cause widespread depletion of the forest and the emission of huge amounts of greenhouse gases. The development of sensitive and reliable fire

detectors and alarm systems is therefore extremely important for the early and successful detection of a fire outbreak, such that these fires can be brought under control and safely extinguished. Such fire detectors could be deployed across various fire-prone sites such as forests, factories, hospitals, schools, universities, banks, shopping malls, and other public places [38].

We have divided this work into two sections in which firstly we optimize the suitable graphitic carbon filler type and concentration, and then cross-compare their roles in regulating thermal, tribological, mechanical, shape switching and recovery properties of PU matrix. We found many unknown phenomena, as can be seen how couple of these fillers largely reduce the strain of PU but one of them behaves differently. We also optimize the concertation and propose that some of the PU properties require low concentration of fillers to enhance the characteristics whereas some of the characteristics require moderate filler concertation to boost the properties of PU, as discussed later in the manuscript. In the second section, we propose two novel embodiments for a heat and fire alarm device: one employing a PU composite SMP that simultaneously acts as a heat sensor and an actuator in combination with an infrared (IR) photosensor as a trigger and another utilizing only the PU composite attached to a metal wire that moves to close an electrical circuit in response to a rise in temperature. These two prototypes successfully detected the presence of heat/fire in laboratory and simulated field environments.

2. Experimental Section

2.1 Materials: Polyurethane (PU) granules (ether type) were commercially purchased. Three different types of graphitic sp^2 carbon, namely 3D graphite (GT), 2D multilayer graphene (MGR), and 1D carbon nanotubes (CNT), were introduced as fillers to develop PU composites.

CNTs were purchased from *SRL, Inc*. MGR with a flake thickness of 11–15 nm was purchased from *Lo-Li. Tec nanomaterials GmbH Germany*. GT powder was purchased from *Labkarts, Chennai, India* (99% purity and -100 mesh).

2.2 Synthesis of PU composites: A twin screw micro-compounder (*Thermo Haake MiniLab 3*), which works on the principle of melt mixing, and an injection molding tool (*Thermo Scientific HAAKE MiniJet Pro Piston*), were employed to prepare PU composites of desired shapes and sizes [39]. To do so, the PU granules were initially washed with ultrapure water and then dried in an oven to remove moisture. During sample processing, the twin screw speed and micro-compounder temperature were maintained at 60 rpm and 200 °C, respectively. After blending for 15 minutes, the mixture was placed inside a cylinder heated to 205 °C. Subsequently, the mixture was fed into the die using a piston at a pressure of 620 bar for 5 seconds, followed by maintaining a post pressure of 400 bar for 15 second. The sample preparation process is illustrated in Figure 1. PU composite samples were prepared by varying the wt% of all fillers, viz. GT, MGR, and CNT, to 0.02%, 0.2%, 1%, and 2%. The composite samples are abbreviated as PUGT, PUMGR, and PUCNT, with C_1, C_2, C_3, or C_4 as the suffix, corresponding to the filler composition of 0.02%, 0.2%, 1%, or 2% wt%, respectively, in the PU matrix.

2.3 Characterizations of the materials and PU composites: The prepared samples were characterized using a range of spectroscopic and microscopic techniques such as Raman spectrophotometry, X-ray diffraction (XRD), field-emission scanning electron microscopy (FESEM), atomic force microscopy (AFM), and Fourier transform infrared (FTIR) spectroscopy. XRD measurements (*Rigaku miniflex Japan*) were performed at 2θ angles of 10^o to 70^o employing Cu K_α radiation (λ = 0.15418 nm) for all the samples. The morphologies of the PU composites were examined using FESEM (*NOVA Nanosem 430*). To do this, cryo-fractured PU composite samples were first prepared. Then, a conductive gold coating was

applied onto the fractured surface to minimize surface charging during sample imaging. AFM measurements (*Asylum Research Cypher*) were performed to investigate the surface topography and roughness of the samples. The RMS roughness was calculated over a scan area of 5 µm × 5 µm. FTIR measurements (*Nicolet iS50, USA*), were performed within a wavenumber range of 4000 cm^{-1} to 400 cm^{-1} to examine the molecular structures, bonding, and functional groups present in the pristine PU and PU composite samples. The thermal properties of pristine PU and PU composite samples were examined using differential scanning calorimetry (DSC, *Mettler Toledo*). The samples weighted 10-15 mg were heated from 20℃ to 230℃ in the first cycle with a heating rate of 20℃/min and then cooled to 10℃ with a cooling rate of 25℃/min. In the second cycle, the heating was done at the same rate up to 230℃. We examined the second heating curve to avoid the thermal stresses in the first cycle. Further, laser flash-based thermal conductivity (*NETZSCH LFA467 Hyper Flash*) tool was employed to measure the thermal conductivity of the samples. Uniaxial tensile tests (*Tinius and Olsen H25KT* universal testing machine) were performed on pristine PU and PU composite samples to estimate various mechanical parameters such as ultimate tensile stress, elongation at break, toughness, and elastic modulus. The tensile tests were performed on dogbone samples prepared *via* melt blending and injection molding using the die standard of ISO 527-2. The repeatability of the results was checked across 8–10 samples. Micro-hardness tests (*Leica VMHT 30A* micro hardness tester) were performed at a load of 50 gf for a dwell time of 10 s on pristine PU and PU composite samples. The micro-hardness tests were performed on disk samples of 20 mm in diameter and 1.5 mm in thickness. The repeatability of the results was checked by measuring at three locations and calculating the average value. Friction and wear measurements were performed on PU and PU composite samples using a rotating ball-on-disk low-load tribometer (*Ducom, India*) under controlled conditions (temperature 24 °C and RH 35%). A stainless-steel ball (hardened chrome steel grade 52100, *Simply Bearings, UK*) 2 mm in diameter was used as

the counterface. The tests were performed on a 2 mm diameter track at a speed of 100 rpm for 1 h, corresponding to 6000 wear cycles. A constant normal load of 1 N was applied throughout the test, and at least three measurements were performed on each sample type. After each test, images of the ball and the sample surface where the test had been conducted were captured using an optical microscope to observe the extent of wear. Dynamic mechanical analysis (DMA) was conducted in a *Perkin Elmer DMA 8000* tool in 3-point bend mode at an oscillation amplitude of 0.2% and a frequency of 1 Hz. The dimensions of the specimen for DMA were 45 mm × 5 mm × 2 mm (length × width × thickness) with a span length of 25 mm. The temperature was varied between 25 ℃ and 80 ℃ with a heating rate of 2 ℃/min. X-ray photoelectron spectroscopy (XPS, *Kratos Axis Ultra*) was carried out on surface-roughened samples to remove any surface oils so that the underlying PU and PU composite material could be probed. Monochromatic Al Kα radiation (hv = 1486.6 eV) was used as the X-ray source. Photoelectrons were acquired from a region of 700 µm × 300 µm on the sample. The pass energy and step size used were 160 eV and 1.0 eV, respectively, for the survey scans and 20 eV and 0.1 eV for the high-resolution C 1s and O 1s scans. During the measurements, an electron flood gun was used to neutralize any surface charges on the samples to prevent sample charging. Ultra-thin sections of the samples were prepared for transmission electron microscopy (TEM) using an ultramicrotome (*Leica Ultracut UCT*). The ultra-thin sections, approximately 150 nm thick, were cut using a diamond knife at room temperature and transferred onto a 200 mesh carbon support copper grid. The sections were imaged using a transmission electron microscope (*FEI Titan*) operating at an accelerating voltage of 200 kV. The BET-specific surface area and pore distribution of samples were determined by N_2 adsorption-desorption analysis using a *Nova Touch LX2* surface area analyzer at a temperature of 77.35 K after an initial degassing pre-treatment of the samples at 200℃ for 4 h.

Thermo-mechanical shape memory tensile tests were performed in a computer-controlled *Tinius and Olsen H25KT* universal testing machine equipped with an environmental chamber [39]. The shape fixity ratio (R_f) and shape recovery ratio (R_r) were calculated using Equations 1 and 2, respectively:

$$R_f = \frac{L_u - L_i}{L_s - L_i} \quad (1)$$

$$R_r = \frac{L_u - L_r}{L_u - L_i} \quad (2)$$

Where L_s is the deformation length, L_u is the fixed length (length at temporary state), L_i is the initial length, and L_r is the recovered length of the sample.

In addition, two different environmental conditions (hot air oven and hot water bath) were used to extensively study the shape memory behavior of PU. The shape memory tests were performed in different environments, each employing the following four-step cycle:

1. Heating the sample at 75 ºC for 10 min
2. Bending the sample to a 30º angle
3. Cooling the sample to 30 ºC (ambient temperature)
4. Heating the sample to 75 ºC to achieve shape recovery

In the hot air environment, a hot air oven was used to perform the tests where the temperature was maintained at 75 ºC before the samples were placed inside. For the hot water environment, a water-filled beaker was heated to 75 ºC using a hot plate before the samples were immersed in the water.

The R_f and R_r values were calculated for these samples using Equations 3 and 4, respectively:

$$R_f = \frac{150^{\circ} - \theta_f}{150^{\circ}} \quad (3)$$

$$R_r = \frac{\theta_r}{150^{\circ}} \tag{4}$$

where θ_f is the angle for the fixed temporary shape after the sample cooling to 30 ºC and θ_r is the angle of the recovered shape after heating at 75 ºC.

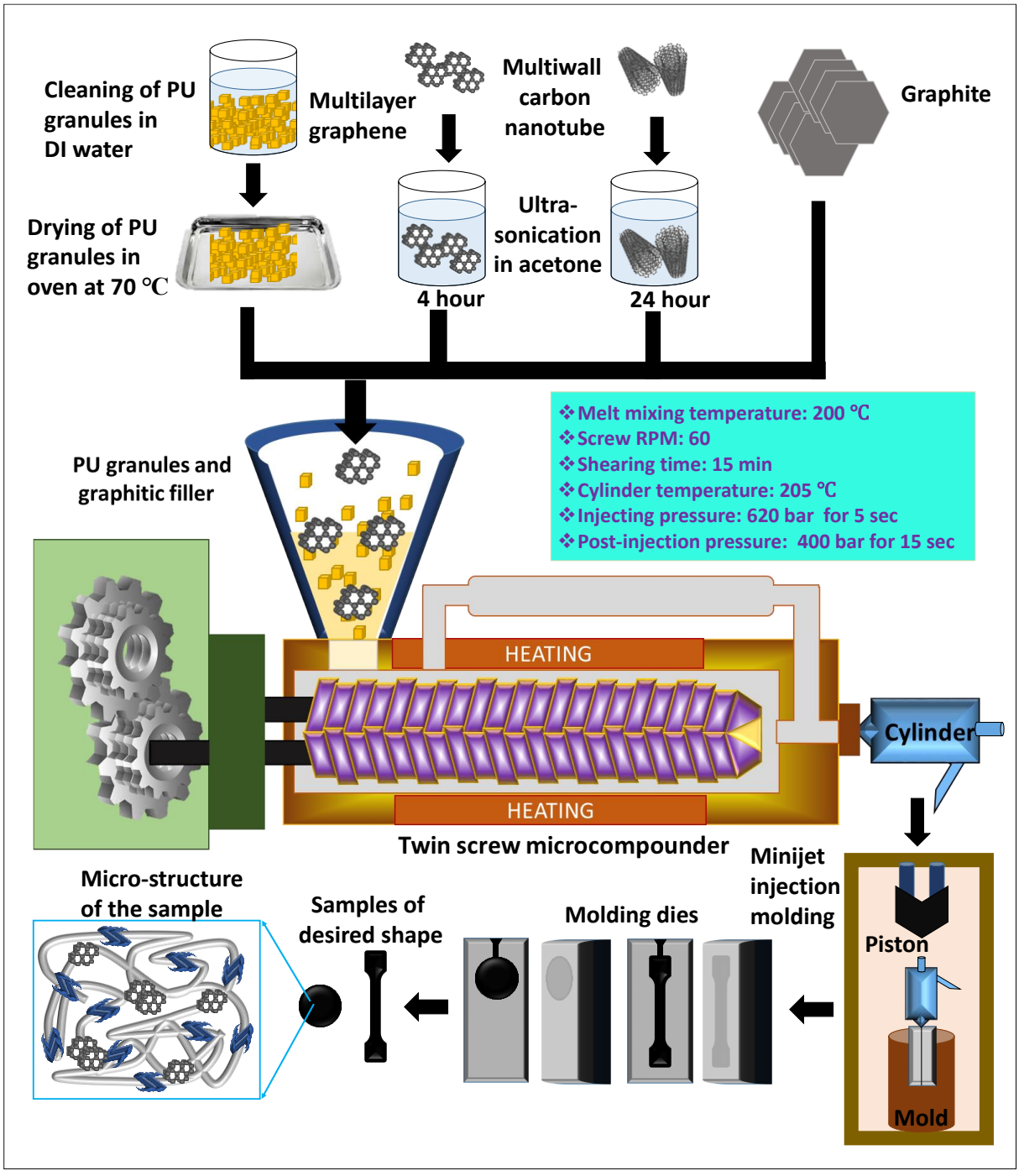

Figure 1: An illustration of the synthesis of PU-composites using micro-compounder along with injection molding tools. Graphitic fillers of different dimensionality were introduced in PU, and samples of different sizes and shapes were prepared for various characterizations.

3. Results and Discussion

3.1. Thermal and shape memory properties

Thermal conductivity (TC) is a key parameter for thermo-responsive SMPs. We first measured the thermal conductivity of pristine PU, PUGT, PUMGR, and PUCNT composites. Figure 2a shows the thermal conductivity of these samples measured at three different temperatures of 25, 50, and 75 °C. It is evident from Figure 2a that the reinforcement by all the graphitic carbons enhances the thermal conductivity of PU at all three temperatures. However, tuning of filler concentration did not significantly alter the thermal conductivity. This suggests that a low concentration of fillers, such as 0.02-0.2 wt%, is sufficient to boost the thermal conductivity of the PU. The improved thermal conduction of PU composites, in comparison to pristine PU, is due to the presence of a conductive filler. The filler increases the conductive pathway between the PU chains and enhances the polymer structure by aligning the polymer chains. As a result, it causes filler-induced crystallization of the PU, which facilitates or accelerates phonon transport [40, 41]. To clearly visualize the advancement of thermal conductivity due to filler introduction, we computed thermal conductivity enhancement (TCE) factor from equation 5

$$\text{TCE}\ (\%) = \frac{\text{TC}_{\text{PU-Composite}} - \text{TC}_{\text{Pristine PU}}}{\text{TC}_{\text{Pristine PU}}} \text{ x } 100 \qquad (5)$$

From Figure 2b, it is evident that the introduction of fillers contributes to TCE by 15 to 55% at different temperatures, which is significant.

Next, cyclic thermo-mechanical tests were performed to investigate and optimize the shape memory characteristics. Figures 2c-2e show the thermo-mechanical stress-strain curves of PU and PU composites. In a typical thermo-mechanical shape memory measurement, the samples were heated above the glass transition temperature, T_g, and were deformed into a temporary shape. This shape could be held upon cooling to ambient temperature. In this process, all the samples store and release the stress/energy *via* a strain effect. The strain energy and the stresses generated at the time of deformation at the elevated temperature are stored in the samples. The graphitic sp^2 carbon fillers aid in improving the shape memory characteristics by interacting with the soft (amorphous) segments present in the PU matrix. This reduces the mobility of the PU chain-like network during the deformation. Thus, when the PU or PU composites are subjected to deformation during the thermo-mechanical tests (at a constant 50% elongation for all the samples), the hindrance in the deformation (strain) of the chain-like network of PU by the fillers can cause higher deformation stresses in PU composites with respect to pristine PU. This behaviour is clearly reflected in Figures 2c-2e, where PU composites generally show higher recoverable stress than pristine PU, especially with higher filler compositions (1–2 wt%). For example, high recovery stresses were found for PUGT-C_4 (1.9 MPa), PUMGR-C_3 (1.3 MPa), and PUCNT-C_4 (1.75 MPa) as compared to pristine PU (0.97 MPa), which translates to ~34–96% enhancement in recoverable stress for the PU composites with respect to pristine PU.

The shape fixity ratio and shape recovery ratio for the first thermo-mechanical stress-strain cycle were extracted and presented in Figures 2f-2g. Optimizing filler composition is paramount to realize adequate recoverable stress with good shape recoverability. Otherwise, the over-enhancement of one of these parameters is likely to cause a degradation of other characteristics of the composite material. While the shape fixity ratio R_f did not follow a clear trend with filler composition (Figure 2f), we mainly focused on the shape recovery ratio R_r.

The reinforcement of graphitic sp^2 carbons and the increase of filler composition had an observable effect on the shape recovery (Figure 2g). At a low reinforcement amount of 0.02–0.2 wt%, the PU composites showed a degree of shape recovery comparable to or higher than pristine PU. However, the shape recovery ratio decreased when the filler composition was increased to 1–2 wt%. With lower graphitic sp^2 carbon loading (0.02–0.2 wt%), the minimal chain restriction in these PU composites, as well as their slightly higher thermal conductivity, enabled their comparable or better shape recoverability than pristine PU. This trend was also observed even at up to three thermo-mechanical cycles, where the PU composites continued to show a higher shape recovery ratio than pristine PU, though increase in number of thermo-mechanical cycle decreased the shape recovery ratio of all type of the samples. (**Supplementary Information 1**). Upon repetitive cycles, the hydrogen bonding between hard segments is primarily broken to a certain extent, and also the repetitive mechanical forces and thermal variation during the cycle can cause chain scission, where the long polymer chains are broken into shorter segments. This can significantly reduce the bond reformation and hence reduce the shape recovery ratio of all the types of samples [42], [43]. Additionally, during the thermomechanical test, the recovery stress is considerably less than the applied programming stress (Figures 2c-2e and Figure S1) which contributes to some unrecoverable shape recovery. Actually, during the programming the generated stresses account for i) stress that leads to the molecular conformational changes (stress relaxation) which is the stored stress, ii) stress that causes mechanical damage, iii) stress that causes unrecoverable permanent deformation, and iv) stress that relates to elastic and viscoelastic deformation [44]. Only stored stress contributes to shape recovery whereas remaining stresses are consumed in permanent deformation, mechanical damage, elastic and viscoelastic deformation, etc., and hence cause reduced shape recovery. However, the presence of graphitic carbon fillers in the PU composites, by interfering with the mobility of the polymer chains, helped to limit the extent of chain degradation, hence

realizing a better shape recovery ratio than pristine PU even after repetitive thermo-mechanical cycling (**Supporting Information 1**).

Next, we examined the shape memory properties in hot air and hot water conditions to discover how the filler composition influences the shape memory characteristics in such environments. Although we did not observe a clear trend in overall shape recovery time when changing the concentration of the fillers in the PUGT, PUMGR, and PUCNT composites, the shape recovery was always faster in these composites than in pristine PU for both hot water and hot air environments (Figure 3a and 3b and Figure 4a and 4b). Figure 3a illustrates the shape recovery of temporarily deformed PU and PU composite samples as a function of recovery time in a hot water environment. The samples were bent to 30° (total deformation of 150°, *i.e.*, the fixed angle was 30°) and had to straighten themselves to 180° for complete shape recovery. Images recorded at recovery angles of ~30°, 90°, 120°, 135°, 150° and 180° are shown in Figure 3a. The tests were repeated, and the average recovery times were extracted for complete shape recovery (*i.e.*, shape recovery from 30° to 180°) for different samples, as shown in Figure 3b. For all PU and PU composite samples, shape recovery behaviour was observed (Figure 3a), and the rate of shape recovery was found to be considerably faster in PUGT, PUMGR, and PUCNT samples compared to pristine PU (Figure 3b). The best shape actuation performance in each family of the sp^2 carbon fillers (GT, MGR, and CNT), in terms of reduction of average recovery time relative to pristine PU, was found to be 36.1% in PUGT-C_4, 46.8% in PUMGR-C_3 and 37.6% in PUCNT-C_1. This indicates that, in a hot water environment, the rate of shape recovery of PU can be increased by ~36–47% after the insertion of multi-dimensional graphitic sp^2 carbons.

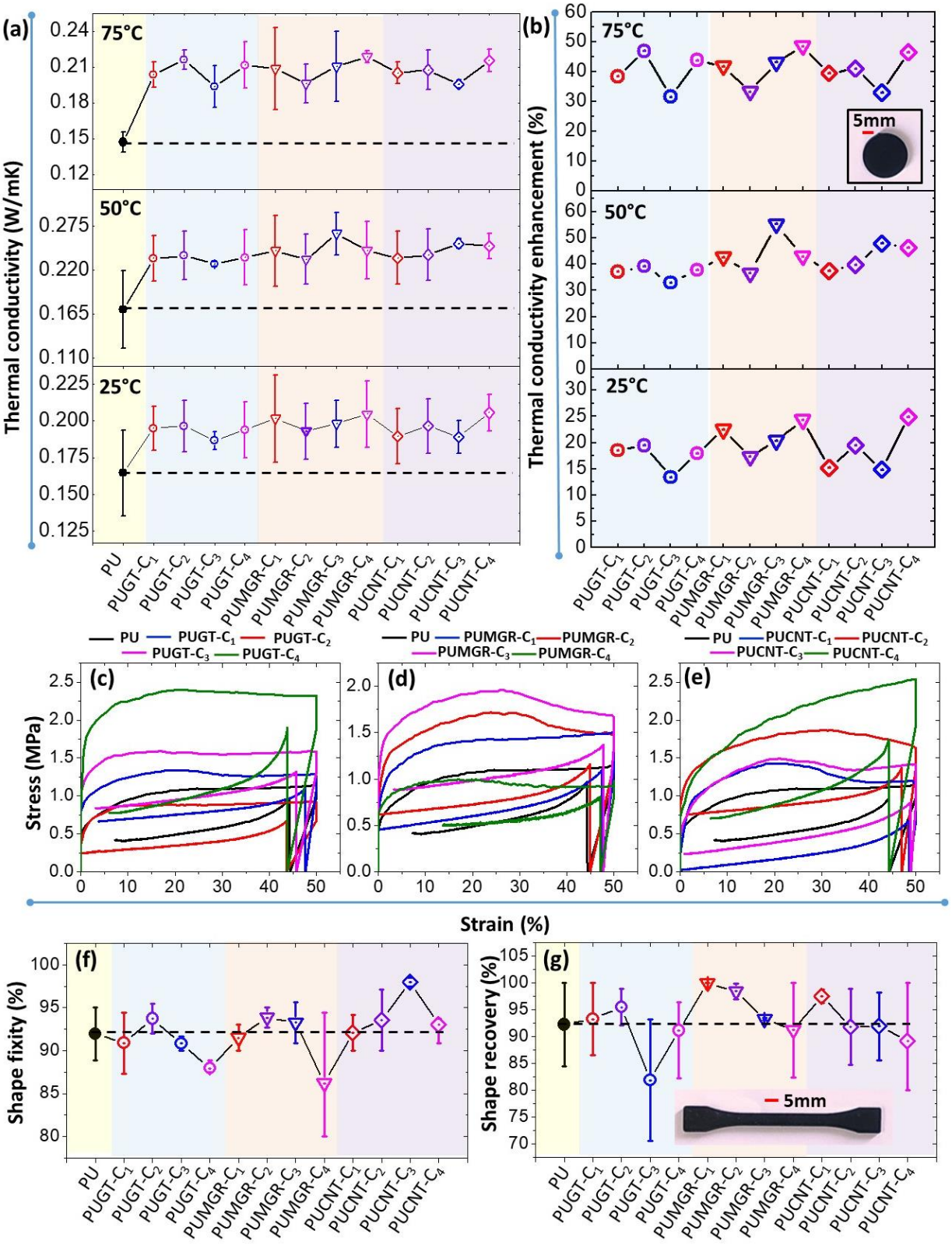

Figure 2: Thermal characterization and shape memory properties of pristine PU and PU composite samples. (a) Average thermal conductivity of pristine PU and PU composites at different temperatures of 25, 50, and 75 °C. (b) Thermal conductivity enhancement of PU composites at different temperatures; inset in (b) represents picture of original sample (to show shape and size) used for thermal conductivity measurements (scale bare represents 5 mm). Representative first-cycle stress-strain curves of (c) PUGT, (d) PUMGR, and (e) PUCNT

composites; the stress-strain curve of pristine PU is included in each graph for comparison purposes. Average (f) shape fixity ratio and (g) shape recovery ratio for the first cycle for all the samples measured after at least three tests on each type of the samples; the dash lines in (f) and (g) indicate the average shape fixity ratio and shape recovery ratio of pristine PU, and included for comparison purpose. The inset in (g) represents picture of original sample (to show shape and size) used for thermo-mechanical tests.

Furthermore, PU composites consistently show faster shape recovery than pristine PU in hot air environments as well (Figures 4a and 4b). In the best PU composite samples of each category (PUGT, PUMGR, and PUCNT), the rate of shape recovery was calculated to be ~20–29% faster than pristine PU (Figures 4a and 4b). The faster shape recovery of the PU composite is attributed to the presence of graphitic sp^2 carbons in the polymer matrix. Bending the samples for shape memory tests results in an inhomogeneous strain distribution between the graphitic sp^2 carbons and the surrounding PU matrix because of the high elastic modulus difference between the reinforcement materials (GT, MGR, and CNT) and the PU matrix. This modulus difference leads to apparent strain-induced crystallization due to strain localization, resulting in PU composites with higher strain energy storage and higher induced stress than pristine PU [45] [46]. Moreover, the presence of graphitic sp^2 carbons provides thermally conducting sites inside the PU matrix. Thus, the combination of higher strain energy stored in the bent state together with the ability of the graphitic carbon fillers to conduct thermal energy more efficiently throughout the PU matrix during heating ensures a faster shape recovery in PU composites than pristine PU. It is expected that with a relatively higher filler loading percentage of 1–2 wt%, there are more thermally-conducting filler sites and a higher stored strain energy compared to a 0.02–0.2 wt% filler loading, hence explaining the relatively faster shape recovery observed with a higher filler loading.

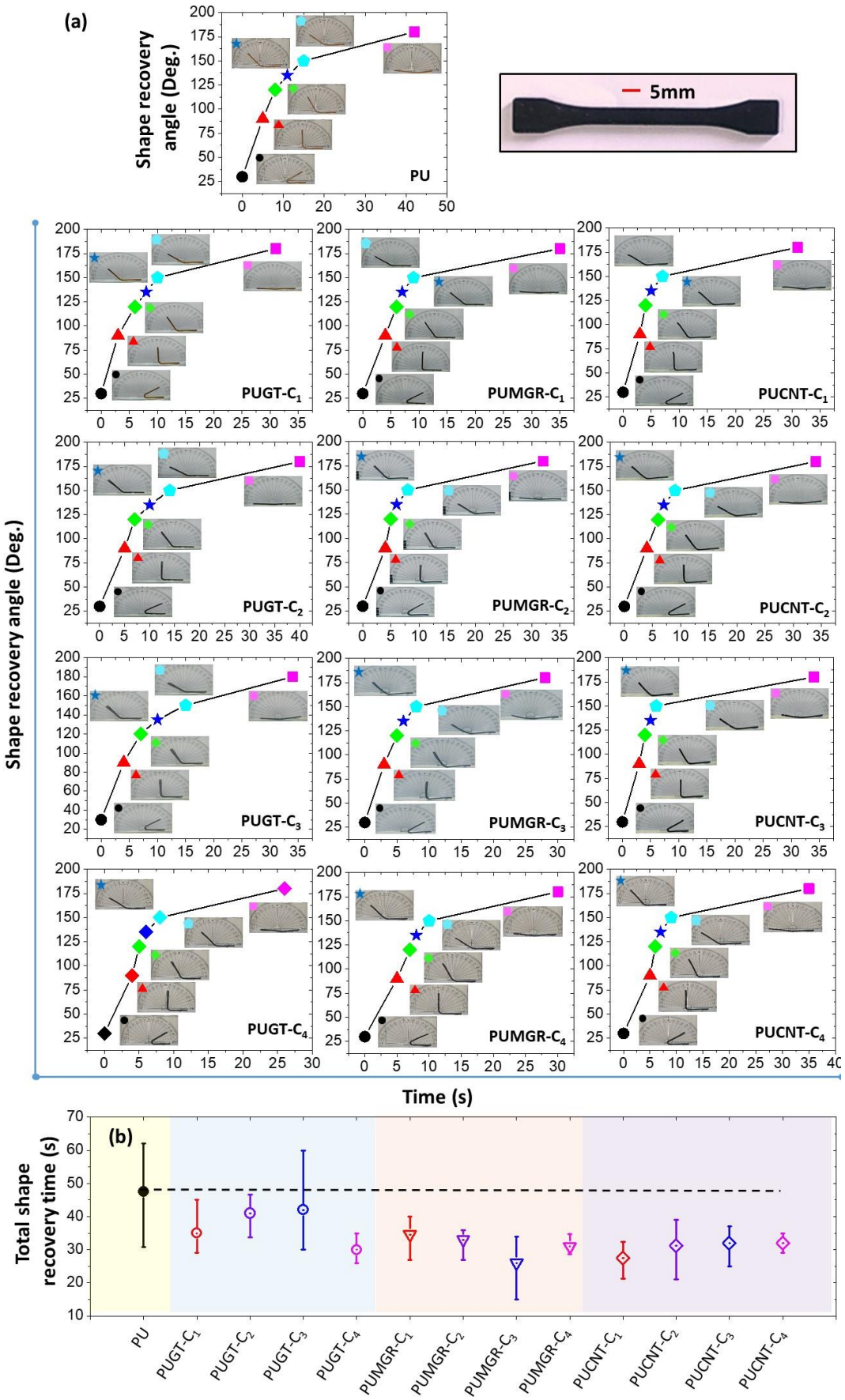

Figure 3: (a) Shape recovery of pristine PU and PU composites as a function of time in the hot water environment, corresponding optical images at different stages of shape recovery are

shown as insets. The picture of original sample used for this test is also included for better understanding of the results. (b) Average shape recovery time for pristine PU and PU composites in the hot water environment; the dashed line indicates the average total recovery time of pristine PU for comparison purposes.

Further, we noticed that the rate of shape recovery of the PU and PU composites depends on the heating environment. When tested in the hot water environment, the rate of shape recovery of the PU and PU composites was faster for the first 80% of the total shape recovery span (*i.e.*, the angle transition from 30° to 150°). Still, it became comparably slower for the remaining 20% of the shape recovery span. The shape recovery rate for the first 80% of the total shape recovery span was measured to be as high as 18.75°/s in PUGT-C_4, 18.75°/s in PUMGR-C_3, and 25°/s in PUCNT-C_3, suggesting that a high filler concentration (1–2 wt%) for all three filler types (GT, MGR and CNT) enables faster shape recovery than lower filler concentrations. The quick release of stored stresses in the initial few seconds in a hot water environment facilitates faster shape recovery in the first 80% of the total shape memory span. In contrast, for the hot air environment, the overall shape recovery time for the PU and PU composites was longer than for the hot water environment, with a relatively linear rate of recovery with time. The hot air environment gave maximum recovery rates of up to 1.7°/s in PUGT-C_4, 1.66°/s in PUMGR-C_4, and 1.6°/s in PUCNT-C_1, suggesting that the release of stored stresses could be slower and more consistent with time in a hot air environment. **Supplementary Movies SM-1 and SM-2** show the shape recovery of the pristine PU and PU composite samples in hot water and hot air environments, respectively.

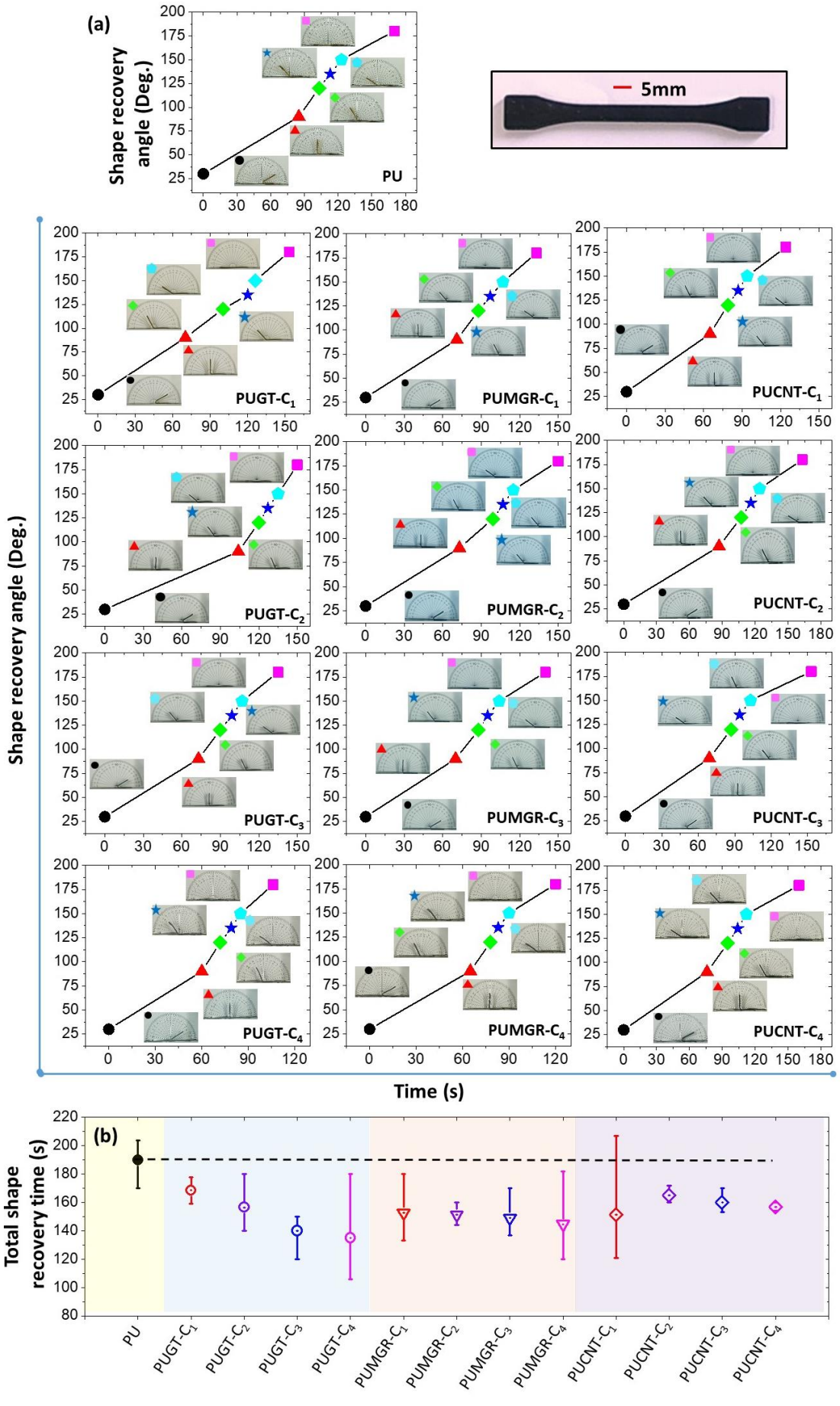
(a)
Shape recovery angle (Deg.)
PU
5mm
PUGT-C1
PUMGR-C1
PUCNT-C1
PUGT-C2
PUMGR-C2
PUCNT-C2
PUGT-C3
PUMGR-C3
PUCNT-C3
PUGT-C4
PUMGR-C4
PUCNT-C4
Shape recovery angle (Deg.)
Time (s)
(b)
Total shape recovery time (s)
PU
PUGT-C1
PUGT-C2
PUGT-C3
PUGT-C4
PUMGR-C1
PUMGR-C2
PUMGR-C3
PUMGR-C4
PUCNT-C1
PUCNT-C2
PUCNT-C3
PUCNT-C4

Figure 4: (a) Shape recovery of pristine PU and PU composites as a function of time in the hot air environment, corresponding optical images at different stages of shape recovery are shown as insets. The picture of original sample used for this test is also included for better understanding of the results. (b) Average shape recovery time for pristine PU and PU composites in the hot air environment; the dashed line indicates the average total recovery time of pristine PU for comparison purposes.

We have also compared the shape memory performance of our PU composite samples with SMPs in literature having different fillers (Table 1). Fan et. al found 81.8% shape recovery in polyurethane during thermo-mechanical cycle test which decreases to 76.4% in the subsequent 3 cycles [47]. Kim et al. fabricated polyurethane/graphene composites and found reduction of shape recovery at higher thermo-mechanical test cycles [48]. Sofla et.al studied the unconstrained shape recovery of polyurethane/graphene composite and concluded that 1 wt% of graphene in polyurethane/graphene composite can lead to high (94±2%) shape recovery [49]. Ebrahimi et al. developed polyurethane-multiwall carbon nanotube (PU/MWCNT) composites with varying concentrations of MWCNTs (0.5, 1, 2, and 5 wt%), and found that the shape recovery ratio of PU/MWCNT composite in a hot water was higher than that of pure polyurethane across all 10 test cycles [50]. They also identified a percolation threshold at a low concentration of 0.5-1 wt%, achieving 100% shape recovery within 25-33 seconds. However, at higher 2 and 5 wt% concentrations, the shape recovery ratio decreased, and the recovery time was increased. Overall, the shape memory performance of our PU composites, in terms of percentage shape recovery and the rate of shape recovery in different environments, was found to be better than many of the previously studied SMPs and SMP composites with different fillers.

Table 1: Shape memory performance of various SMPs and SMP composites from literature.

Polymer	**Parameters:** **Medium for shape recovery,** **Number of cycles tested,** **Maximum shape recovery achieved (%),** **shape recovery time (sec)**	**Reference**
Polyurethane	Thermo-mechanical, 3 cycles, up to 81.8%	[47]
Poly vinyl alcohol/carbon nanotube composite	Thermo-mechanical, 1 cycle, 54%	[51]
Polystyrene based	Thermo-mechanical, 4 cycles, up to 70%	[52]
Polyurethane/graphene composite	Thermo-mechanical, up to 98.6%	[53]
Polyurethane/graphene composite	Thermo-mechanical, 4 cycles, up to 98.0%	[48]
poly(methyl methacrylate)/ poly(ethylene glycol) composite	Air, 3 cycles, up to 95.0–97.0%, 50 s	[54]
Acrylate/carbon black composite	Thermo-mechanical, 4 cycles, up to 95.0%, 2110 s	[55]
Polyurethane/multiwall carbon nanotubes	Water, 10 cycles, up to 90.0%, 68 s	[50]
Epoxy	Air, above 90.0%, 400 s	[56]
Polyvinyl alcohol/graphene oxide composite	Air, 10.0%, 3600 s	[57]
	Water, up to 100.0%, 50 s	
Epoxy/carbon nanotubes composite	Air, 100.0%, 1700 s	[58]
Polyvinyl alcohol/glutaraldehyde composite	Water, 100.0%, 35 s	[59]

Epoxy	Thermo-mechanical free recovery, 4 cycles, up to 100.0%, 960 s	[60]
Polyurethane/graphene	Up to 100.0%	[49]
Trans-1,4-polyisoprene/chopped carbon fibre composite	Air, up to 100.0%	[61]
Polyurethane/polystyrene/ acidic functionalized Multiwall CNT	Air, up to 100.0%, 14 s	[62]
Polycaprolactone and polyethylene glycol cross-linked/cellulose nanocrystals composite	Water, up to 86.0%, 350 s	[63]
Polyurethane/graphite, multilayer graphene, CNT composite	Thermo-mechanical, 3 cycles, up to 100.0%	This work
	Air, 3 cycles, up to 100.0%, 106 s	
	Water, 3 cycles, up to 100.0%, 14 s	

3.2. Friction and wear

Next, we investigated the sliding friction and wear properties of engineered PU. The frictional curves for PUGT, PUMGR, and PUCNT samples are shown in Figures 5a-5c, with the frictional curve of pristine PU included in each figure for comparison purposes. The average coefficient of friction (COF) of each sample type, extracted from the steady-state region of the curves of at least 3–4 tests (***see*** **Supplementary Information 2** for details), is shown in Figure 5d. Pristine PU shows an average COF of ~0.3, which is higher than the average COF of the PU composites. A closer examination of the data revealed that 0.2 wt% was the critical concentration for each type of graphitic sp^2 carbon filler, beyond which the COF was drastically reduced. A similar trend was also observed in the wear characteristics of the samples, where the graphitic sp^2 carbon fillers considerably reduced the wear damage of PU (Figure 5e). The pristine PU shows severe wear, as confirmed by a wide and severe wear track as well as

significant wear debris transferred to the ball. The PU-steel tribo-pair is representative of a soft-hard tribo-system. When PU starts to slide under the hard steel counterface, wear damage occurs due to abrasion, ploughing, and elastic-plastic deformation. On the other hand, when multi-dimensional graphitic sp^2 carbon fillers were introduced into the PU matrix at low filler concentrations, there was a negligible change in the wear behavior, as can be seen from the significant damage in 0.02 to 0.2 wt% GT, MGR, and CNT reinforced PU. However, when the filler concentration was increased to 1–2 wt%, a huge reduction in the wear damage and friction was realized, as seen from the narrower and fainter wear tracks, smaller amount of debris transfers to the ball, as well as a 50–66% reduction in the COF in the C_3 and C_4 PU composites.

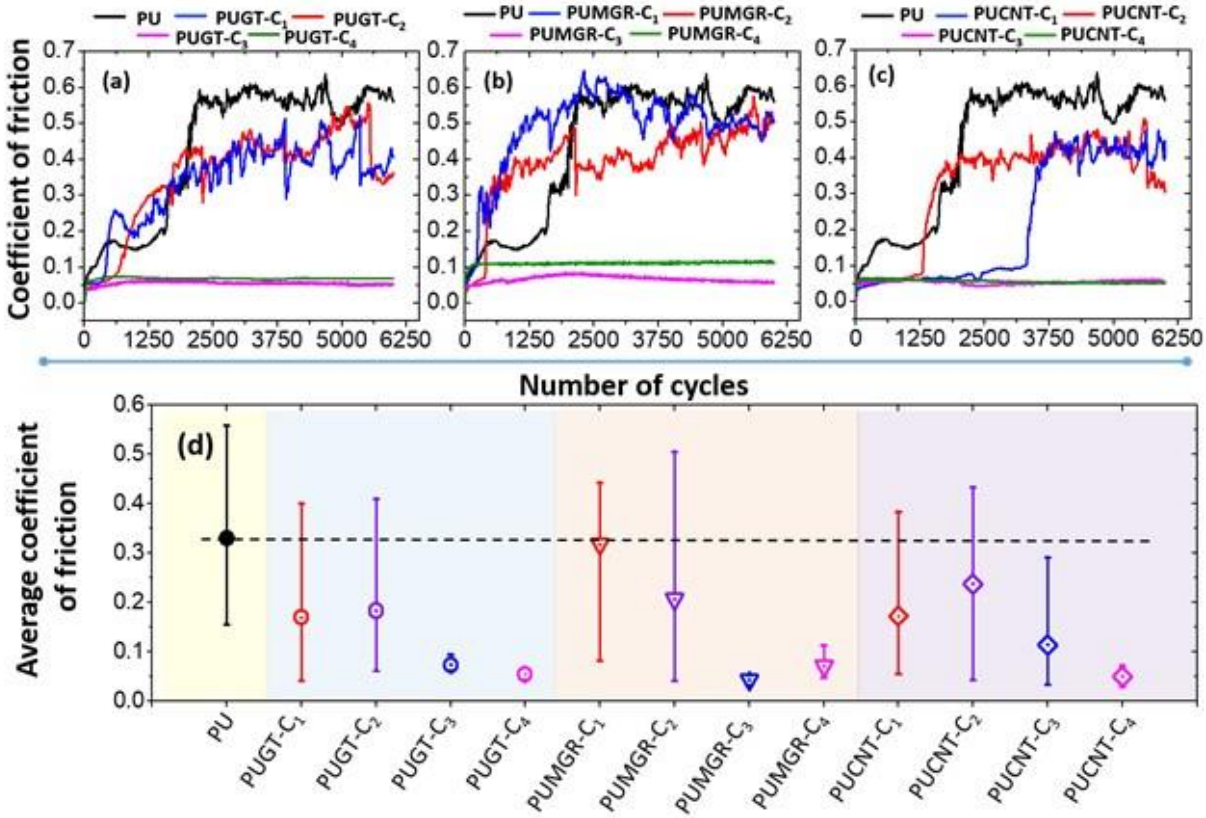

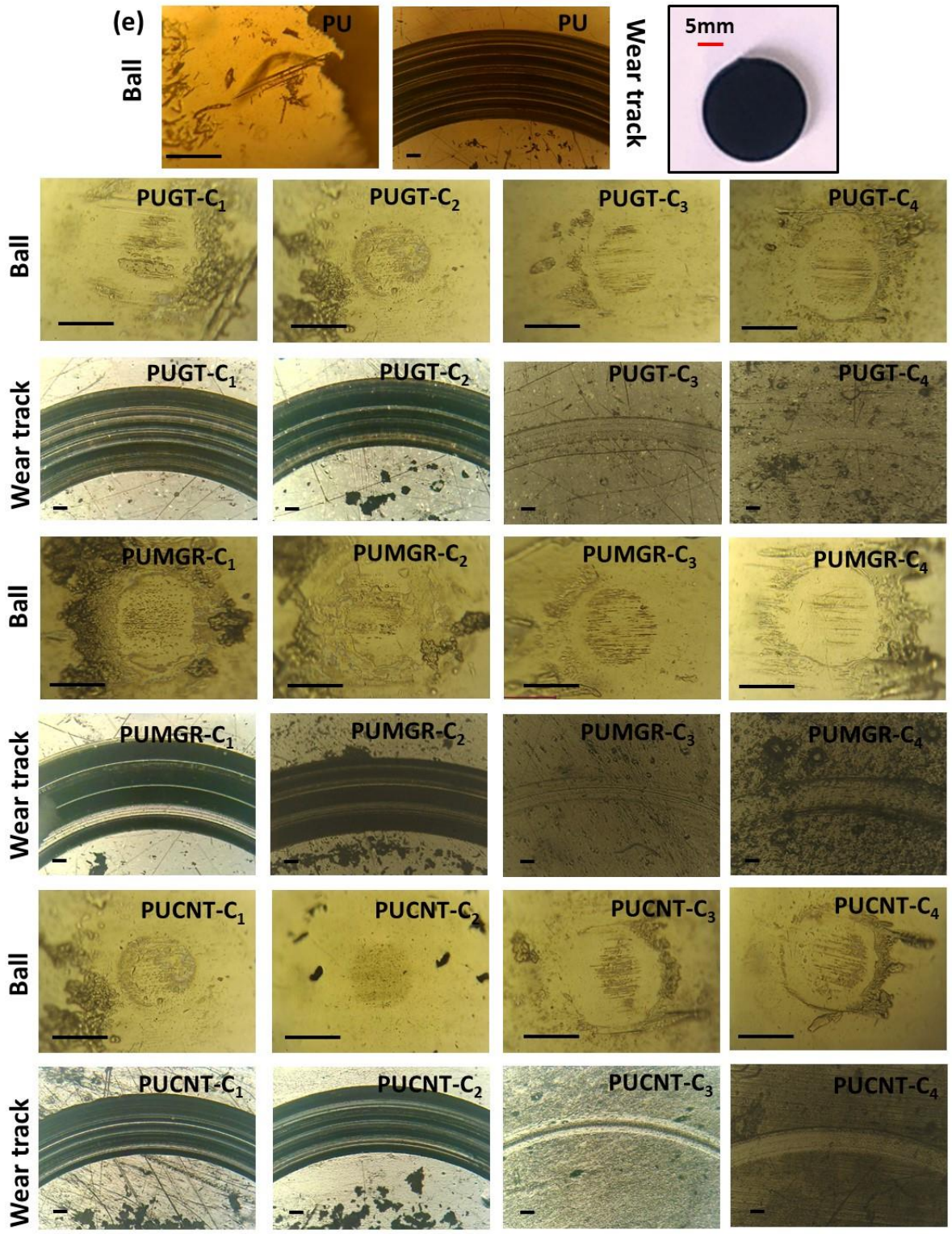

Figure 5: Friction and wear behavior of pristine PU and PU composites. Representative coefficient of friction (COF) curves for (a) PUGT, (b) PUMGR, and (c) PUCNT composites; the coefficient of friction cycle of pristine PU is included in each graph for comparison purposes. (d) Average COF of each type of sample measured after at least 3–4 measurements; the dashed line indicates the average COF of pristine PU for comparison purposes. (e) Corresponding optical images of the balls and wear tracks after the ball-on-disk tribological measurements. The scale bars in the ball and wear track optical images represent 20 μm and

50 µm, respectively. The picture of original sample used for tribological test is also included for better understanding of the results, the scale bar in the sample picture represents 5 mm.

In graphitic sp^2 carbons, the sp^2-bonded monoatomic layers are coupled by weak van der Waals interactions. In GT and MGR, the graphene sheets are stacked on top of one another, whereas in MWCNTs, the rolled graphene cylinders are stacked on top and adjacent to one another. The predominant lubricating mechanisms in graphitic carbons are due to the ease of shearing of the weakly-bonded sp^2-carbon layers (graphitic carbon layers are coupled by weak van der Waals forces) and water intercalation between the graphitic carbon layers [64], where water molecules enter and reside in between the layers of graphitic carbon. As a result, water intercalation weakens the surface basal plane interactions and facilitates the shearing of the basal plane. Since the measurements were performed at a relative humidity (RH) of 35-40%, there is a high likelihood of water intercalation occurring, which facilitated the easy shearing of graphitic carbons and thus enabled the low friction observed in the PU composites reinforced with graphitic carbons (PUGT, PUMGR, and PUCNT samples) at the optimum filler concentration (≥ 1 wt% based on the friction data). At the same time, the excellent mechanical properties of the fillers, especially MGR and CNT, contributed to alleviating the wear of the PU composites.

3.3. Mechanical properties and wettability

The graphitic carbon fillers and their concentrations also played a role in modifying the mechanical and surface wettability properties of PU. Tensile tests were performed on the PU and PU composites to obtain various mechanical parameters such as ultimate tensile strength (UTS), toughness, elastic modulus, and elongation at break, which could be estimated from the stress-strain curves, Figure 6a-6h. The stress-strain curves of PU, PUGT, PUMGR, and PUCNT composites are shown in Figure 6a-6c. Pristine PU exhibited an average UTS of ~58.8 MPa (Figure 6d), toughness ~118.49 MPa (Figure 6e), elastic modulus ~1089 MPa (Figure 6f), and strain before break of ~323.16% (Figure 6g). The introduction of ~1–2 wt%

GT and MGR slightly enhanced the UTS but at the expense of significantly reducing the maximum strain or stretchability. The 3D and 2D nature of the GT and MGR reinforcement fillers acts as obstacles between the PU polymer chains, thus hindering chain re-organization. At a higher filler concentration of ~1–2 wt%, the fillers occupy more sites within the PU matrix, and the mobility of the PU polymer chains gets reduced. Furthermore, self-aggregation of the fillers promotes the concentration of stresses at these locations, which can ultimately cause a ductile-to-brittle-like transition. What's interesting is that higher CNT concentrations (~1–2 wt%) did not significantly degrade the stretchability of PU, unlike the GT and MGR type fillers. We postulate that the 1D structure of CNTs allows them to align with the chain-like polymeric network of PU and, therefore, does not lead to significant filler aggregation. Additionally, the high surface area (*see* **Supplementary Information 3**) of the CNT fillers could enable a greater degree of intermolecular interactions between the CNT and the PU chains. Consequently, the stresses in PUCNT composites do not easily concentrate at a certain point; instead, the CNTs and PU chains align themselves along the stretching direction in which the tensile stress is applied [65, 66]. This results in a higher maximum strain in PUCNT composites than in the PUGT and PUMGR composites at high filler concentrations. It should be noted that lower concentrations (0.02–0.2 wt%) of GT or MGR fillers do not significantly change the elongation at the break of the PU in tensile tests due to the dominance of the PU matrix over the small amount of fillers. The elastic moduli (Figure 6f) of the PU composites were generally higher than pristine PU, although the extent of enhancement was not very large. However, the introduction of the fillers degraded the toughness of PU, especially at higher filler concentrations (Figure 6e). Generally, a higher elastic modulus contributes to a higher recoverable stress [67]. This trend was found to be true for our PU composite samples in the thermo-mechanical shape recovery tests. Additionally, the PU composites did not show a clear trend in the modification of indentation hardness with filler concentration (***see*** **Supplementary**

Information 4). However, some PU composite samples showed considerably higher hardness than pristine PU.

Since the surface wettability characteristic indicates the type of surface forces/surface energy acting on the samples that assist in understanding friction and wear properties, we also performed contact angle measurements **(Supplementary Information 4).** The hydrophobic character was observed to be significant at higher graphitic carbon filler concentrations (1 and 2 wt%) Figure S4. In these graphitic carbon-based fillers, the polar component of the surface energy is contributed by the availability of surface functional groups (hydroxyl, carbonyl, carboxyl, and ether) [68]. In contrast, the dispersive component is contributed by non-polar dispersive forces such as van der Waals forces [69]. Thus, introducing graphitic-carbon fillers reduces the polar component and the PU composite's surface-free energy.

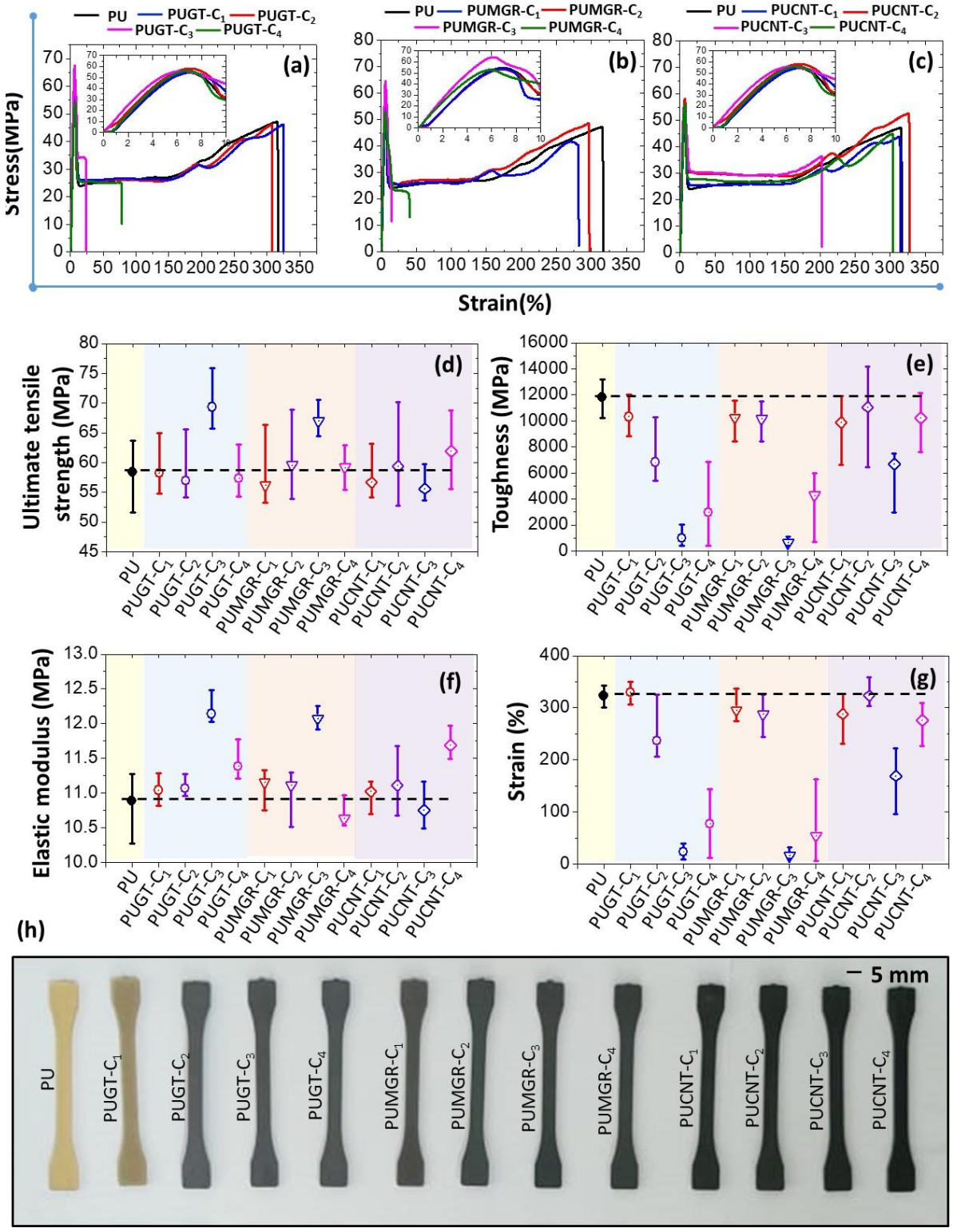

Figure 6: Mechanical properties of pristine PU and PU composites. Representative stress-strain curves of (a) PUGT, (b) PUMGR, and (c) PUCNT composites; the stress-strain curve of pristine PU is also included in each graph for comparison purposes. Average (d) ultimate tensile strength, (e) toughness, (f) elastic modulus, and (g) maximum strain of pristine PU and PU composites extracted from multiple stress-strain curves. The dashed lines in (d)-(g) represent the respective values measured for pristine PU and are indicated in the graphs for comparison purposes. (h) Images of real PU and PU composite samples used for tensile measurements.

3.4. Material characterization and morphologies

The PU and PU composite samples were characterized by FTIR, XRD, and DSC to probe the interaction of the multi-dimensional graphitic sp^2 carbon fillers with the PU matrix and analyze the various types of bonding, phases, and thermal characteristics. FTIR spectra in Figures 7a-7c show the characteristic CONH, C=O, C–H, and N–H bonds of PU in all the PU and PU composite samples, which indicate that at all the filler concentrations, the structure of biphasic (hard and soft phases) PU is not altered, and hence the PU composites are also expected to maintain shape memory characteristics [70, 71]. XRD spectra in Figures 7d-7f reveal the characteristic crystallographic peaks of the graphitic sp^2 carbon fillers, particularly the <002> peak, that indicate their presence within the PU composite samples.[72] DSC measurements in Figures S5a-S5c suggest that the application of graphitic sp^2 carbon fillers does not affect the glass transition temperature (T_g) of the PU (***see*** **Supplementary information 5** for detailed description of FTIR, XRD, and DSC measurements). We extended the characterization by performing DMA measurements on pristine PU and PU composites in order to better understand their material systems and functional properties. DMA measurements were performed in the temperature range of 23 to 80℃ on pristine PU and PU composites containing 0.2 wt% GT, MGR, and CNT fillers, and the storage modulus and damping factor (Tan δ) were estimated (Figures 7g-7h). At temperature, $T < T_g$, a slight increase in the storage modulus of PU composites compared to pristine PU is due to an increase in the π-π interactions and van der Waals interactions between the GT, MGR, and CNT fillers and the PU chains. As the temperature increased above the T_g, the storage modulus sharply decreased due to energy dissipation during the transition from the glassy to the rubbery state. The Tan δ peaks (which were used to determine the T_g) were found to occur at 53.7℃, 54.3℃, 53.9℃, and 52.8℃ for pristine PU, PUGT-C_2, PUMGR-C_2, and PUCNT-C_2 samples, respectively. The very similar T_g

values between PU and the PU composites show that the graphitic sp^2 carbon fillers had a negligible effect on modifying the T_g of PU, which is in agreement with the DSC results.

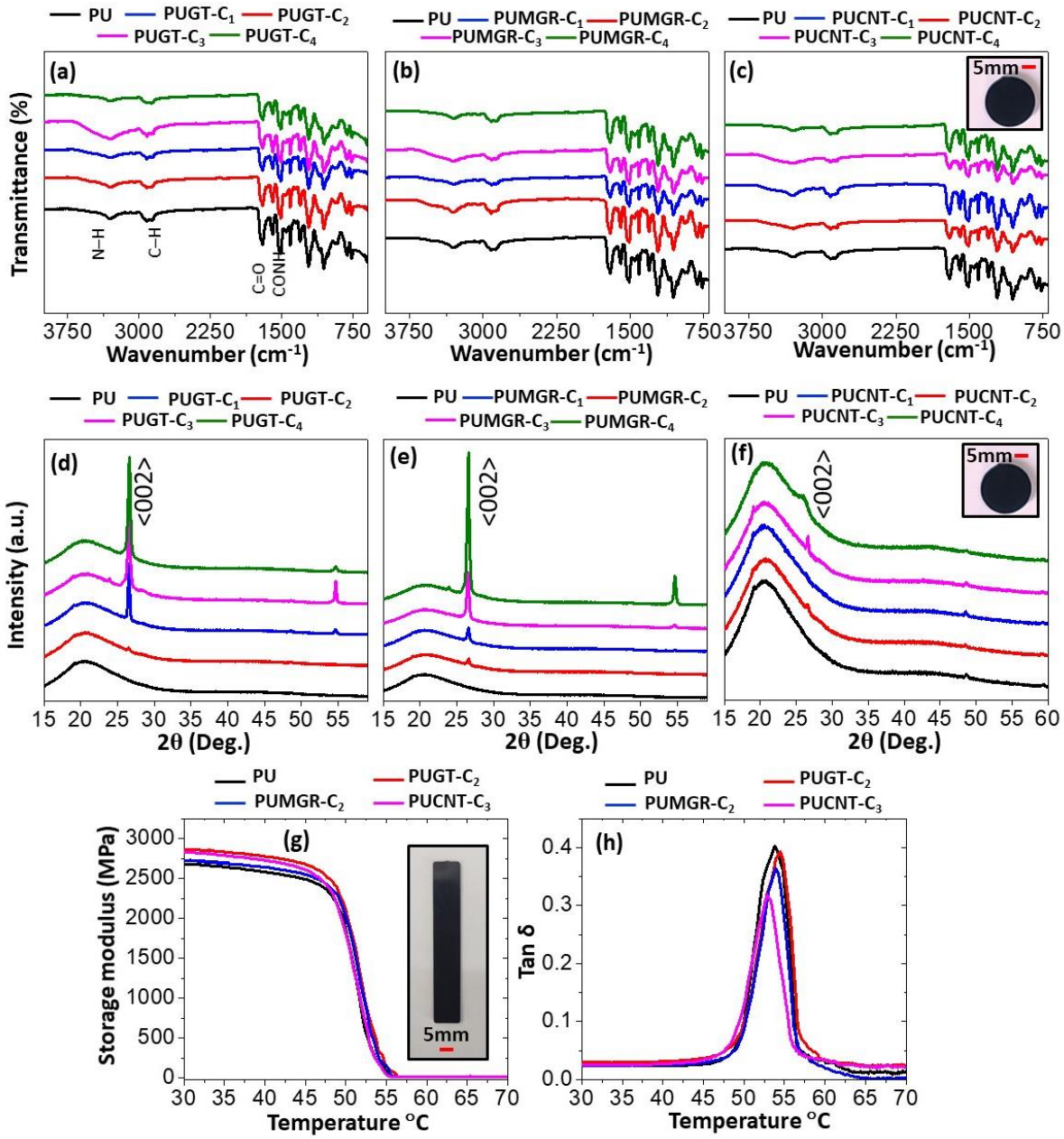

Figure 7: Spectroscopic and thermal characterizations of pristine PU and PU composites. (a)-(c) FTIR, (d)-(f) XRD, for PU, PUGT, PUMGR, and PUCNT samples. Results for (g) storage modulus, and (h) damping factor (Tan δ) with temperature for pristine PU, PUGT-C_2, PUMGR-C_2, and PUCNT-C_2 samples, extracted from DMA measurements. Insets of (c), (f) and (g) represent real sample images used for FTIR, XRD and DMA measurements.

To understand the effect of the sp^2 carbon filler type and its concentration on the respective PU composite's fracture mechanisms, we comprehensively examined the

morphology of these samples (cryo-fractured samples) using FESEM. Figures 8a- 8m show the FESEM images of cryo-fractured PU and PU composites at different filler concentrations. The images clearly reveal that the fracture morphology was significantly changed after the introduction of the fillers. The FESEM images of pristine PU (Figure 8a) indicate a more elongated and rubber-like fracture that gave a smooth fractured surface morphology as visualized in the zoomed-in image (***see*** **Supplementary information 6**). As PU is an elastomer, it is expected to undergo a large degree of elastic deformation before failure, and the observed fracture morphology reflects its expected failure mechanism. However, the PU composites loaded with GT and MGR reveal rougher fracture surfaces and brittle-like fractures at higher filler concentrations (Figures 8b-8m). The roughness of the fractured PU composite surface loaded with CNT was found to be somewhat in between that of pristine PU and MGR/GT loaded PU composites, even at higher concentrations. This suggests that the 1D geometry of the CNT favors maintaining a higher stretchability of the PUCNT composite as compared to the PUGT and PUMGR composites. Next, we attempted to examine the nanostructures of pristine PU and the PU composites using TEM. Figures 8n-8t show the TEM images of PU and PU composites with different fillers (at 0.2 wt% filler concentration). The structures of each type of filler (GT, MGR, and CNT) could be clearly seen in the amorphous PU matrix, particularly for those fillers that were aligned out-of-plane such that their graphitic sp^2 carbon layered structures were revealed. Graphite flakes/particles were observed for the PUGT composite, sheet-like structures of MGR were observed in the PU-MGR composite, and tubular structures of CNT were observed in the PUCNT composite. The average inter-planar distances for the graphitic sp^2 carbon fillers were measured to be 0.325 nm, 0.324 nm, and 0.326 nm for GT, MGR, and CNT fillers, respectively, consistent with the XRD analysis. TEM images also revealed a large difference in size between the GT/MGR fillers and the CNT fillers. While the size of the GT and MGR fillers was on the order of 1 μm or more, the average length

of the CNTs was around 100–200 nm, which is an order of magnitude less. The larger size of the GT/MGR fillers could, therefore, also have been a key factor in restricting the mobility/stretchability of the PUGT and PUMGR composites, whereas the smaller CNT fillers would have a much smaller effect. Furthermore, the surface topography of the samples was examined using AFM that shows addition of graphitic fillers to the pristine PU matrix resulted in the formation of noticeable bumps on the surface (**see Supplementary information 7**, Figure S7 for detailed description).

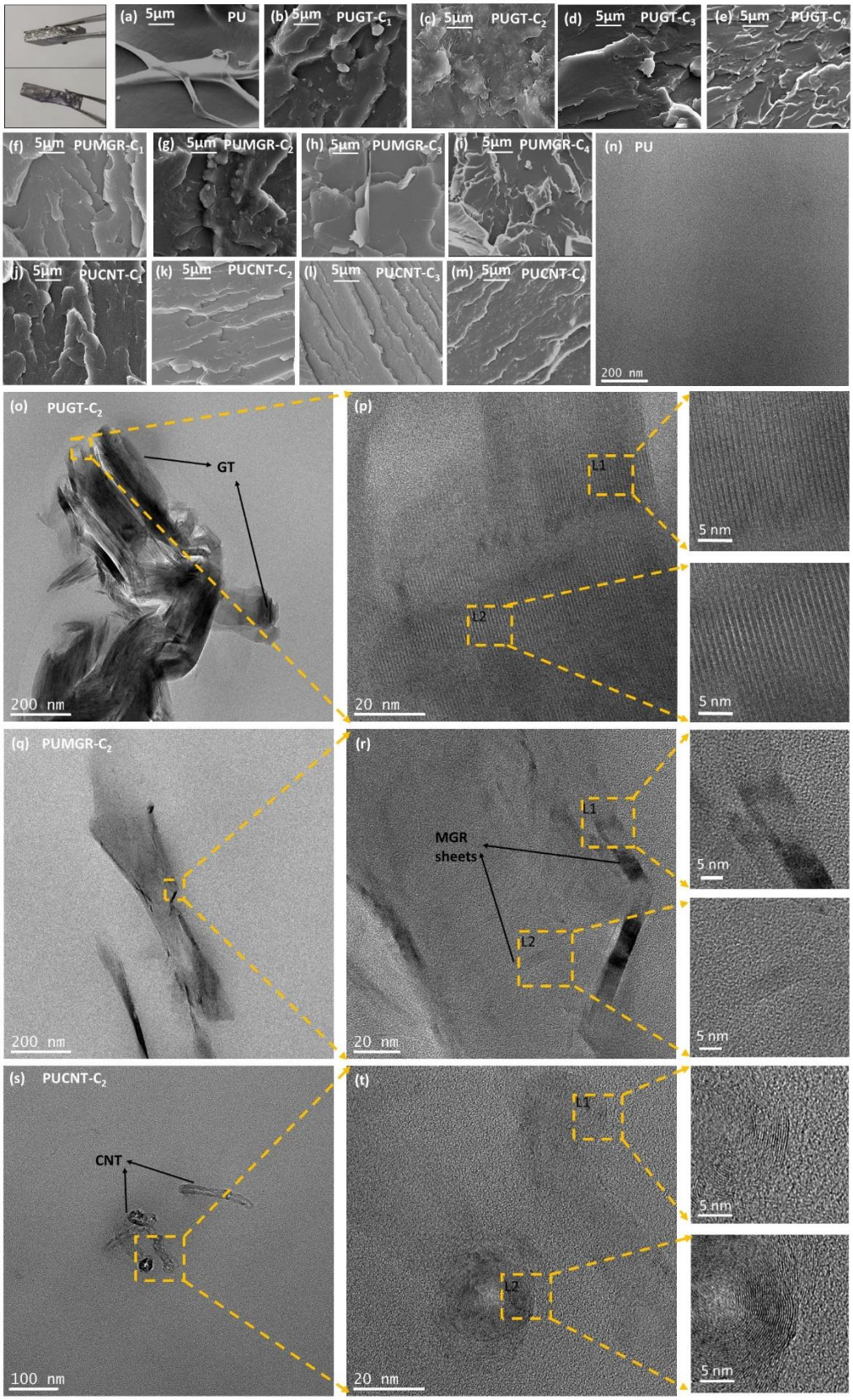

Figure 8: (a)-(m) Morphological characterizations of the cryo-fractured surfaces of pristine PU and PU composites using FESEM, image of real cyro factured surface is enclosed in the start. FESEM images of the cryo-fractured surfaces of (a) pristine PU, (c)-(e) PUGT composites, (f)-

(i) PUMGR composites, and (j)-(m) PUCNT composites. TEM images of (n) pristine PU, (o)-(p) PUGT-C_2 composite, (q)-(r) PUMGR-C_2 composite, and (s)-(t) PUCNT-C_2 composite captured at different magnifications.

XPS was performed to probe the bonding environment in PU and PU composites containing 0.2 wt% graphitic carbon fillers (***see*** **Supplementary information 8, S**upplementary Figures S8a-S8d). High-resolution C 1s spectra revealed a peak at ~284.8 eV in PU [73], which was shifted to a lower binding energy in the PU composites. This was due to the introduction of graphitic fillers with a lower binding energy position of around 284.0–284.4 eV for graphitic sp^2 carbon [74], compared to the carbon peak at 284.8 eV, which is representative of polymeric carbon. This indicated the reinforcement effect of graphitic carbon materials in the PU matrix. The graphitic carbon reinforcement effect was also found to be present in O 1s spectra, where the peak positions for PUGT, PUMGR, and PUCNT samples were slightly altered with respect to pristine PU.

3.5 Heat and Fire alarm devices

In the final part of our work, we employed the PU composite in two novel designs of heat/fire alarm devices: a first embodiment with hybrid technologies of shape memory and infrared (IR) photodetection for smoke, heat, and fire detection and a second embodiment with shape memory technology but no IR photo-detection capability for only heat and fire detection. In both device designs, PUGT-C_4 composite was used as SMP component that acted as a heat sensor as well as an actuator. Concurrently, in the first embodiment, an infrared (IR) photo-transmitter and a photodetector were employed in the device to trigger the alarm by breaking the light circuit/signal. Figures 9a-9g show the first embodiment of a smoke, heat, and fire alarm device design with a schematic illustration of the device and how it would function in

the laboratory and simulated field environments. In this device, the pre-deformed PU composite element is placed near the photo-transmitter and photodetector (Figure 9a). In the event of heat/fire, a couple of reactions are possible. In the case where the fire results in the generation of smoke, the accumulation of smoke particles between the photo-transmitter and photo-detector will disturb/scatter the IR radiation, causing the IR photo-circuit to be broken and thereby activating the alarm (Figure 9b). Similarly, when the temperature rises in the event of heat/fire, the pre-deformed PU composite element will sense the heat and start to actuate (Figures 9c-9d) as soon as the temperature reaches close to/above the T_g (~55 °C). Upon actuation/shape recovery, the PU composite element acts as a barrier between the photo-transmitter and the photodetector, blocking the IR radiation to the photo-detector and thus activating the alarm (Figures 9c-9d). As a proof-of-concept, we made a device prototype based on the first embodiment and tested it under the aforementioned conditions. Figure 9e is a photograph showing the activation of the hybrid SMP PU composite and photo-diode heat/fire alarm device upon its exposure to smoke. Figure 9f is a photograph showing the activation of the hybrid alarm device upon its exposure to a dry heat laboratory environment. Finally, Figure 9g is a photograph showing the activation of the hybrid alarm device upon its exposure to fire in a simulated field environment.

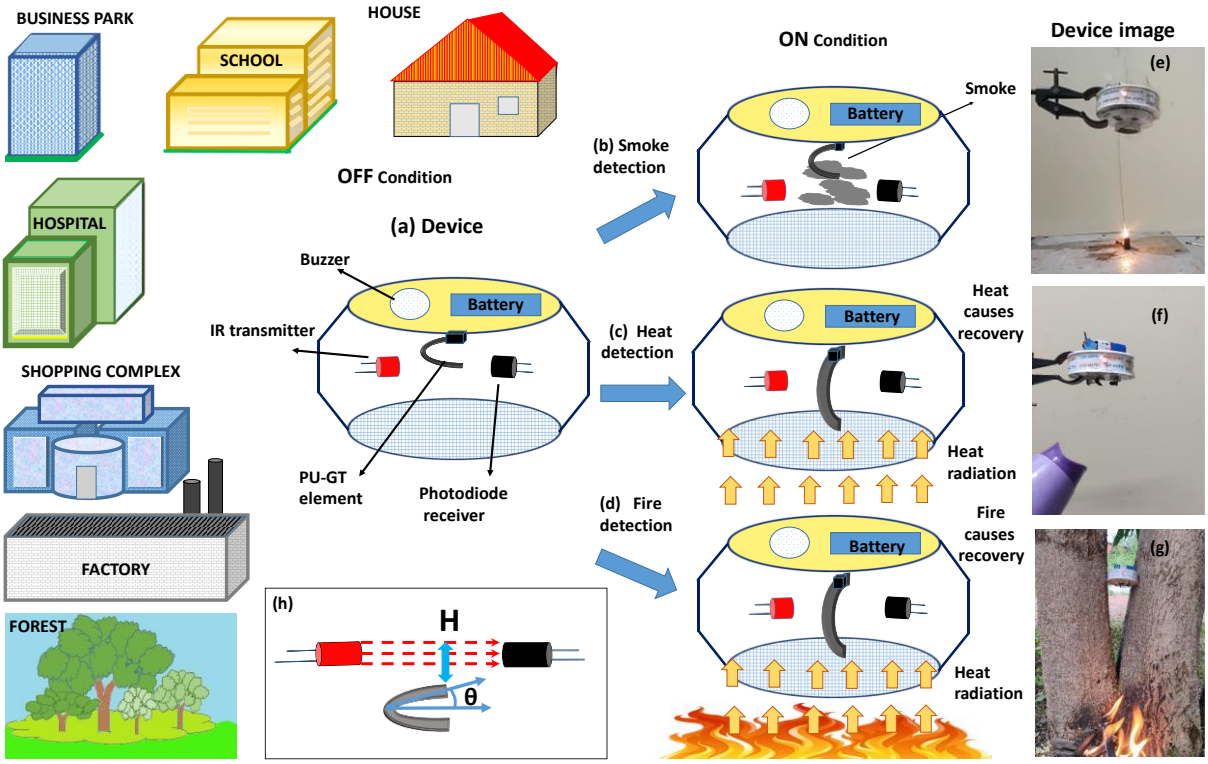

Figure 9: Heat/fire alarm based on the hybrid shape memory polymer composite/IR photodiode concept: first embodiment. (a) Device schematic, (b-d) activation conditions of alarm in case of smoke, heat, and fire respectively, (e-g) device demonstration in simulated field environments for smoke, heat, and fire respectively. (h) Demonstration of how alarm blow time depends on H and θ parameters of the device for fire and heat.

Figures 10a-10g show the second embodiment of a heat and fire alarm device design with a schematic illustration of the device and how it would function in the laboratory and simulated field environments. In this second embodiment, the PU composite element is deformed to a temporary U-shape and is placed between electrodes 1 and 2 (Figure 10a). One of the arms of PU composite which is attached to electrode 1 is fixed, while the other arm near electrode 2 is free for actuation. An electrically conducting wire connected to electrode 1 is also deformed to a U-shape and placed on the deformed U-shaped PU composite. Since the wire is not connected with electrode 2 in normal conditions, the whole circuit will be in the open circuit state, *i.e.*, the alarm will be switched OFF. When the temperature rises due to heat/fire and reaches close to/above the T_g, the PU composite element actuates, and the free arm holding the conducting wire touches electrode 2, leading to the closure of the circuit and

activation of the alarm (Figures 10b-10c). Figure 10d is a photograph showing the operation of the device based on the second embodiment upon its exposure to dry heat in a laboratory environment. Figures 10e-10f are photographs showing the operation of the device based on the second embodiment upon its exposure to fire in a simulated field environment. **Supplementary Movies SM-3 and SM-4** show the operation of these device prototypes based on the first and second embodiments in different environments. The devices work efficiently in different simulated environments.

Additionally, in both the embodiments, the alarm blow time depends on the bent extent of the PU-composite element (i.e. angle between the two arms of the PU-GT element, θ), and distance H. Thus, θ varies inversely to H. We have illustrated this in Figures 9h and 10g. In the first embodiment, Figure 9h, H is the distance between the IR light path (photo-sensor and detector) and SMP-based movable arm. In the second embodiment, Figure 10g, H is the distance between SMP's movable arm and the second electrode. For θ equal to θi° (Initial angle), the time taken to cover H will be maximum. Thus, for the alarm to go off fast, the H should be minimal.

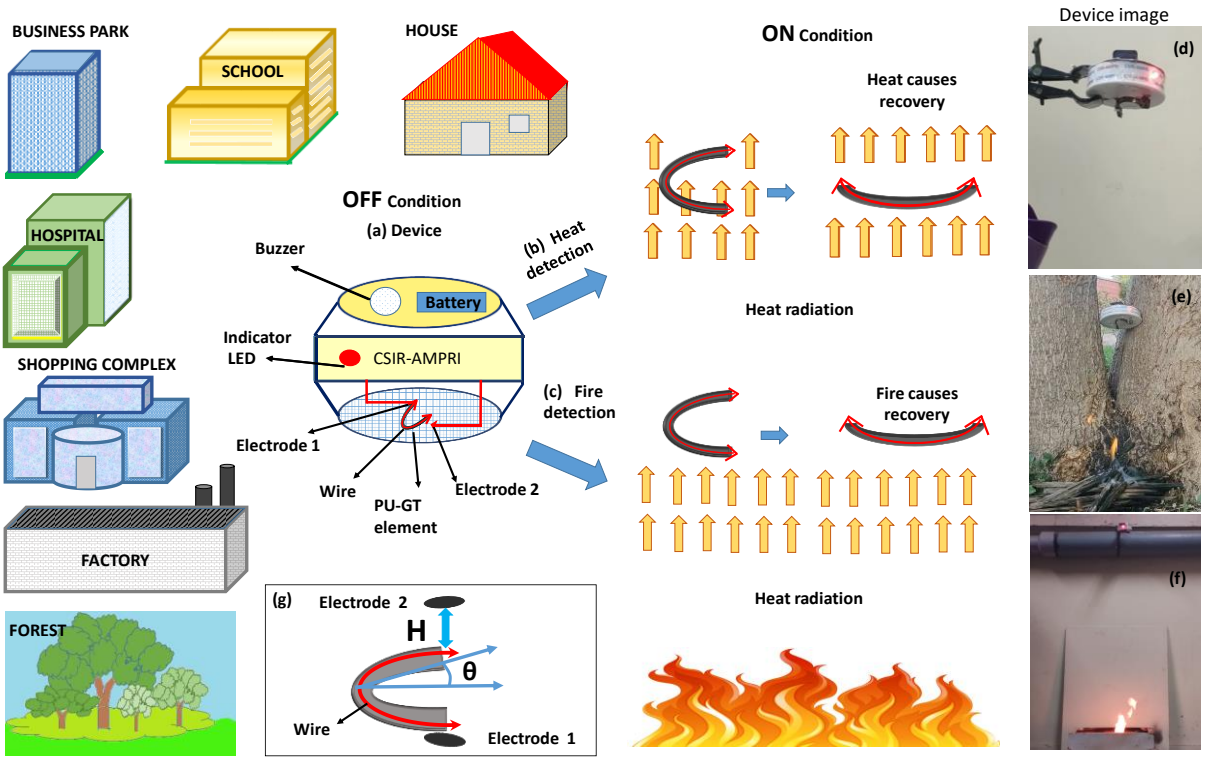

Figure 10: Heat/fire alarm based on shape memory polymer composite: second embodiment. (a) Device schematic, (b-c) activation conditions of alarm in case of heat and fire respectively, (e, d-f) device demonstration in simulated field environments for heat, and fire respectively. (g) Demonstration of how alarm blow time depends on H and θ parameters of the device for fire and heat.

4. Conclusions

In summary, we have investigated the roles of three types of multi-dimensional graphitic carbon fillers, namely GT, MGR, and CNT, in controlling the shape memory, tribological, and other functional properties of PU. In doing so, we have uncovered how the filler type and concentration can be used to tune the various properties of the resultant PU composite. Our findings suggest that

- A low concentration of fillers (0.02–0.2 wt%) is sufficient to enhance the thermal conduction and shape recovery ratio while maintaining/marginally altering the PU's flexibility. Moreover, thermal conductivity enhancement factor of PU composite shows 15 to 55% increment, compared to pristine PU. On the other hand, a higher filler

concentration (1–2 wt%) is useful for obtaining faster shape recovery up to 100% with ~34–96% enhancement of stress recovery.

- A relatively higher filler concentration (1–2 wt%) in PU helps to significantly enhance the wear resistance and large reduction of COF by 50–66%, compared to pristine PU.
- We also notice that the application of multi-dimensional graphitic carbon fillers in PU could modify the tensile, wettability (contact angle enhancement up to 21.6%), and hardness characteristics, compared to pristine PU.
- Finally, we design and fabricate two embodiments of novel heat/fire alarm device prototypes; one based on a hybrid shape memory effect and IR photodiode concept, and another without an IR photodiode but utilizing the PU composite (PU-GT composite in particular) as the heat-sensing and actuating element by harnessing its shape memory effect. We demonstrate that the device prototypes in embodiments could work successfully for fire and heat detection in the laboratory as well as in simulated field environment tests, signalling that they could potentially be further developed for commercial use as an integrated smoke, heat, and fire detector.

Acknowledgments

This research is supported by the Council of Scientific and Industrial Research (CSIR), India, through the project MLP 303. J.V. acknowledges CSIR, India, for providing financial support through the GATE-JRF fellowship. The authors wish to thank Prof. Pratima Solanki from Jawaharlal Nehru University, New Delhi, India; Dr. P. Asokan, Dr. M. K. Gupta, Dr Gaurav Gupta, Dr. M. Shafeeq, Dr. D. P. Mondal, Mr. A. Khare, Mr. D. Kashyap and Mr. N. Prashant, from CSIR-Advanced Materials and Processes Research Institute, Bhopal, India; for their help.

Authors contributions:

Jeet Vishwakarma: Designed the research project. Prepared the samples and performed the characterizations. Wrote the initial draft of the manuscript.

Shubham Jaiswal: Helped in characterizations. Critically reviewed the manuscript and helped to improve the manuscript draft.

Chetna Dhand: Helped in characterizations. Provided constructive inputs on experimental results analysis. Critically reviewed the manuscript and helped to improve the manuscript draft.

Reuben J. Yeo: Helped in characterizations. Provided constructive inputs on experimental results analysis. Critically reviewed the manuscript and helped to improve the manuscript draft.

Hui Ru Tan: Helped in TEM characterization. Provided constructive inputs on experimental results analysis. Critically reviewed the manuscript and helped to improve the manuscript draft.

Rajeev Kumar: Helped in characterizations. Provided constructive inputs on experimental results analysis. Critically reviewed the manuscript and helped to improve the manuscript draft.

Pradip Kumar: Helped in characterizations. Provided constructive inputs on experimental results analysis. Critically reviewed the manuscript and helped to improve the manuscript draft.

Narendra Singh: Provided constructive inputs on experimental results analysis. Critically reviewed the manuscript and helped to improve the manuscript draft.

Alka Mishra: Provided constructive inputs on experimental results analysis. Critically reviewed the manuscript and helped to improve the manuscript draft.

Ajay Naik: Provided constructive inputs on experimental results analysis. Critically reviewed the manuscript and helped to improve the manuscript draft.

A. K. Srivastava: Provided constructive inputs on experimental results analysis. Critically reviewed the manuscript and helped to improve the manuscript draft.

Neeraj Dwivedi: Conceived the research idea. Designed the research project. Helped in characterizations. Provided constructive inputs on experimental results analysis. Critically reviewed the manuscript and helped to improve the manuscript draft.

Funding:

This research is supported by Council of Scientific and Industrial Research (CSIR), India through the project MLP 303.

Conflict of Interest

The authors declare that they have no conflict of interest

Data Availability Statement

The data that support the findings of this study are available on request from the corresponding author.

References

1. Wang K, Jia Y-G, Zhao C, Zhu XX (2019) Multiple and two-way reversible shape memory polymers: Design strategies and applications. Progress in Materials Science 105. doi:10.1016/j.pmatsci.2019.100572
2. Luo L, Zhang F, Wang L, Liu Y, Leng J (2024) Recent Advances in Shape Memory Polymers: Multifunctional Materials, Multiscale Structures, and Applications. Advanced Functional Materials 34 (14):2312036. doi:https://doi.org/10.1002/adfm.202312036
3. Wang X, He Y, Liu Y, Leng J (2022) Advances in shape memory polymers: Remote actuation, multi-stimuli control, 4D printing and prospective applications. Materials Science and Engineering: R: Reports 151:100702. doi:https://doi.org/10.1016/j.mser.2022.100702
4. Thakur S (2017) Shape memory polymers for smart textile applications. Textiles for advanced applications:323-336
5. Huang H, Han L, Wang Y, Yang Z, Zhu F, Xu M (2019) Tunable thermal-response shape memory bio-polymer hydrogels as body motion sensors. Engineered Science 9 (12):60-67
6. Chen C-T, Liao P-S (2023) Additive design and manufacturing of a quadruped robot actuated by electrothermal effect of shape memory polymer. Sensors and Actuators A: Physical 357:114401. doi:https://doi.org/10.1016/j.sna.2023.114401
7. McEvoy MA, Correll N (2015) Materials science. Materials that couple sensing, actuation, computation, and communication. Science 347 (6228):1261689. doi:10.1126/science.1261689
8. Alapan Y, Karacakol AC, Guzelhan SN, Isik I, Sitti M (2020) Reprogrammable shape morphing of magnetic soft machines. Science advances 6 (38):eabc6414
9. Liu Jessica AC, Gillen Jonathan H, Mishra Sumeet R, Evans Benjamin A, Tracy Joseph B Photothermally and magnetically controlled reconfiguration of polymer composites for soft robotics. Science Advances 5 (8):eaaw2897. doi:10.1126/sciadv.aaw2897
10. Yuan J, Neri W, Zakri C, Merzeau P, Kratz K, Lendlein A, Poulin P (2019) Shape memory nanocomposite fibers for untethered high-energy microengines. Science 365 (6449):155-158. doi:10.1126/science.aaw3722
11. Oladapo BI, Kayode JF, Akinyoola JO, Ikumapayi OM (2023) Shape memory polymer review for flexible artificial intelligence materials of biomedical. Materials Chemistry and Physics 293:126930. doi:https://doi.org/10.1016/j.matchemphys.2022.126930
12. Ze Q, Kuang X, Wu S, Wong J, Montgomery SM, Zhang R, Kovitz JM, Yang F, Qi HJ, Zhao R (2020) Magnetic Shape Memory Polymers with Integrated Multifunctional Shape Manipulation. Adv Mater 32 (4):e1906657. doi:10.1002/adma.201906657
13. Bai Y, Liu J, Ju J, Chen X (2021) Novel Near-Infrared Light-Induced Triple-Shape Memory Composite Based on Poly(ethylene-co-vinyl alcohol) and Iron Tannate. ACS Applied Materials & Interfaces 13 (19):23011-23019. doi:10.1021/acsami.1c05166
14. Song Y, Lai H, Jiao X, Cheng Z, Kang H, Zhang D, Fan Z, Xie Z, Wang Y, Liu Y (2022) Amphibious superlyophobic shape memory arrays with tunable wettability in both air and water. Advanced Composites and Hybrid Materials 5 (2):788-797. doi:10.1007/s42114-021-00363-5
15. Ur Rehman H, Chen Y, Hedenqvist MS, Li H, Xue W, Guo Y, Guo Y, Duan H, Liu H (2018) Self-Healing Shape Memory PUPCL Copolymer with High Cycle Life. Adv Funct Mater 28 (7):1704109. doi:https://doi.org/10.1002/adfm.201704109
16. Zuo X, Zhang X, Qu L, Miao J (2023) Smart Fibers and Textiles for Personal Thermal Management in Emerging Wearable Applications. Advanced Materials Technologies 8 (6):2201137. doi:https://doi.org/10.1002/admt.202201137
17. Lewis CL, Meng Y, Anthamatten M (2015) Well-Defined Shape-Memory Networks with High Elastic Energy Capacity. Macromolecules 48 (14):4918-4926. doi:10.1021/acs.macromol.5b00763
18. Gao H, Li J, Liu Y, Leng J (2021) Shape memory polymer solar cells with active deformation. Advanced Composites and Hybrid Materials 4 (4):957-965. doi:10.1007/s42114-021-00263-8

19. Jing X, Wei J, Liu Y, Song B, Liu Y (2020) Deployment analysis of aramid fiber reinforced shape-memory epoxy resin composites. Engineered Science 11 (2):44-53
20. Constante G, Apsite I, Auerbach P, Aland S, Schonfeld D, Pretsch T, Milkin P, Ionov L (2022) Smart Mechanically Tunable Surfaces with Shape Memory Behavior and Wetting-Programmable Topography. ACS Appl Mater Interfaces. doi:10.1021/acsami.2c01078
21. Zhang D, Wang X, He Y, Feng Y, Cheng Z, Song Y, Hu D, Liu Y (2022) Self-restoration of Underwater Low Adhesive Superoleophobicity on Shape Memory Polymer Arrays. Engineered Science 17:343-350
22. Hu J, Zhang C, Ji F, Li X, Han J, Wu Y (2016) Revealing the morphological architecture of a shape memory polyurethane by simulation. Sci Rep 6:29180. doi:10.1038/srep29180
23. Wu T, Chen B (2017) Facile fabrication of porous conductive thermoplastic polyurethane nanocomposite films via solution casting. Scientific reports 7 (1):1-11
24. Yang H, Shi R, Jiang Q, Ren J (2023) Properties and mechanism of two-way shape memory polyurethane composite under stress-free condition. Advanced Composites and Hybrid Materials 6 (1):1-12
25. Guo Y, Chen Y, Yu Q, Liu H, Li H, Yu Y (2023) Ultra-tough and stress-free two-way shape memory polyurethane induced by polymer segment "spring". Chemical Engineering Journal 470:144212. doi:https://doi.org/10.1016/j.cej.2023.144212
26. Yoonessi M, Shi Y, Scheiman DA, Lebron-Colon M, Tigelaar DM, Weiss R, Meador MA (2012) Graphene polyimide nanocomposites; thermal, mechanical, and high-temperature shape memory effects. ACS nano 6 (9):7644-7655
27. Jaiswal S, Vishwakarma J, Bhatt S, Karak S, Bharti P, Dhand C, Kumar R, Kumar P, Saifullah MSM, Saha S, Mishra R, Dwivedi N (2023) Layered Titanium Carbide-Mediated Fast Shape Switching and Excellent Thermal and Electrical Transport in Shape-Memory-Polymer Composites for Smart Technologies: MAX Versus MXene. Advanced Engineering Materials 25 (17):2300233. doi:https://doi.org/10.1002/adem.202300233
28. Zhao R, Kang S, Wu C, Cheng Z, Xie Z, Liu Y, Zhang D (2023) Designable Electrical/Thermal Coordinated Dual-Regulation Based on Liquid Metal Shape Memory Polymer Foam for Smart Switch. Advanced Science 10 (8):2205428. doi:https://doi.org/10.1002/advs.202205428
29. Kwon Y-J, Park J-B, Jeon Y-P, Hong J-Y, Park H-S, Lee J-U (2021) A Review of Polymer Composites Based on Carbon Fillers for Thermal Management Applications: Design, Preparation, and Properties. Polymers 13 (8). doi:10.3390/polym13081312
30. Kannan RR, Sivabharathy M, Lenin N (2022) Shape memory effect of CuxAl1-xnitinol/MWCNT nanocomposites for actuators in MEMS. Sensors and Actuators A: Physical 334:113327. doi:https://doi.org/10.1016/j.sna.2021.113327
31. Abolhasani D, Moon B, Kang N, VanTyne CJ, Moon YH High-Performance Cu-Al Shape Memory Alloy in Ternary Combination with Graphene Fabricated by Powder Bed Fusion Process. Available at SSRN 4340960
32. Wang QZ, Han FS, Wu J, Hao GL (2005) Thermal stresses in a macroscopic graphite particulates reinforced CuAlMn shape memory alloy studied by internal friction. Materials Science and Engineering: A 408 (1):247-254. doi:https://doi.org/10.1016/j.msea.2005.08.010
33. Wu J, Wang H, Su Z, Zhang M, Hu X, Wang Y, Wang Z, Zhong B, Zhou W, Liu J, Xing SG (2017) Highly Flexible and Sensitive Wearable E-Skin Based on Graphite Nanoplatelet and Polyurethane Nanocomposite Films in Mass Industry Production Available. ACS Applied Materials & Interfaces 9 (44):38745-38754. doi:10.1021/acsami.7b10316
34. Rana S, Cho JW, Tan LP (2013) Graphene-crosslinked polyurethane block copolymer nanocomposites with enhanced mechanical, electrical, and shape memory properties. RSC ADVANCES 3 (33):13796-13803. doi:10.1039/c3ra40711j
35. L. Fonseca B, Fonseca MA, A. Oliveira MS (2018) Thermo-mechanical characterization of shape-memory polyurethane nanocomposites filled with carbon nanotubes and graphene nanosheets. Polym Compos 39 (S2):E1216-E1223. doi:https://doi.org/10.1002/pc.24760

36. Luo J, Shi C, Yin L, Gong K, Qian X, Zhou K (2023) Killing three birds with one stone: A novel regulate strategy for improving the fire safety of thermoplastic polyurethane. Composites Part A: Applied Science and Manufacturing 168:107491. doi:https://doi.org/10.1016/j.compositesa.2023.107491
37. Zhang X, Hu J, Yang Q, Yang H, Yang H, Li Q, Li X, Hu C, Xi Y, Wang ZL (2021) Harvesting Multidirectional Breeze Energy and Self-Powered Intelligent Fire Detection Systems Based on Triboelectric Nanogenerator and Fluid-Dynamic Modeling. Adv Funct Mater 31 (50):2106527. doi:https://doi.org/10.1002/adfm.202106527
38. Zhang M, Wang M, Zhang M, Yang C, Li Y, Zhang Y, Hu J, Wu G (2019) Flexible and Thermally Induced Switchable Fire Alarm Fabric Based On Layer-by-Layer Self-Assembled Silver Sheet/Fe3O4 Nanowire Composite. ACS Applied Materials & Interfaces 11 (50):47456-47467. doi:10.1021/acsami.9b18858
39. Vishwakarma J, Jaiswal S, Bharti P, Dhand C, Kumar R, Hashmi SAR, Srivastava AK, Dwivedi N (2022) Competing and decisive roles of 1D/2D/3D sp2-carbons in controlling the shape switching, contact sliding, and functional properties of polymers. Materials Today Chemistry 25:100960. doi:https://doi.org/10.1016/j.mtchem.2022.100960
40. Kwon YJ, Park JB, Jeon YP, Hong JY, Park HS, Lee JU (2021) A Review of Polymer Composites Based on Carbon Fillers for Thermal Management Applications: Design, Preparation, and Properties. Polymers (Basel) 13 (8). doi:10.3390/polym13081312
41. Varenik M, Sertchook H, Eden E, Buzaglo M, Nir Y, Regev O Effects of Filler Size and Crystallinity on Thermal Performance and Flammability of Polymer Nanocomposites. Carbon Nanostructures: Fundamentals to Applications. AIP Publishing LLC. doi:10.1063/9780735423114_004
42. Wang M, Liang S, Gao W, Qin Y (2022) The effect of promoting hydrogen bond aggregation based on PEMTC on the mechanical properties and shape memory function of polyurethane elastomers. Royal Society Open Science 9 (3):211393. doi:10.1098/rsos.211393
43. Suman T, Jinlian H (2017) Polyurethane: A Shape Memory Polymer (SMP). In: Faris Y (ed) Aspects of Polyurethanes. IntechOpen, Rijeka, p Ch. 3. doi:10.5772/intechopen.69992
44. Shojaei A, Li G (2014) Thermomechanical constitutive modelling of shape memory polymer including continuum functional and mechanical damage effects. Proceedings of the Royal Society A: Mathematical, Physical and Engineering Sciences 470 (2170):20140199. doi:10.1098/rspa.2014.0199
45. Koerner H, Price G, Pearce NA, Alexander M, Vaia RA (2004) Remotely actuated polymer nanocomposites—stress-recovery of carbon-nanotube-filled thermoplastic elastomers. Nature Materials 3 (2):115-120. doi:10.1038/nmat1059
46. Gall K, Dunn ML, Liu Y, Stefanic G, Balzar D (2004) Internal stress storage in shape memory polymer nanocomposites. Applied Physics Letters 85 (2):290-292
47. Fan W, Zhang Y, Li W, Wang W, Zhao X, Song L (2019) Multi-level self-healing ability of shape memory polyurethane coating with microcapsules by induction heating. Chem Eng J 368:1033-1044. doi:10.1016/j.cej.2019.03.027
48. Kim JT, Kim BK, Kim EY, Park HC, Jeong HM (2014) Synthesis and shape memory performance of polyurethane/graphene nanocomposites. Reactive and Functional Polymers 74:16-21. doi:https://doi.org/10.1016/j.reactfunctpolym.2013.10.004
49. Lotfi Mayan Sofla R, Rezaei M, Babaie A, Nasiri M (2019) Preparation of electroactive shape memory polyurethane/graphene nanocomposites and investigation of relationship between rheology, morphology and electrical properties. Composites Part B: Engineering 175:107090. doi:https://doi.org/10.1016/j.compositesb.2019.107090
50. Ebrahimi AH, Sahebian S (2022) Influence of functional carbon nanotube and multi-cyclic shape memory performance on thermally triggered polyurethane nanocomposites. Polymer Composites 43 (12):8925-8934. doi:https://doi.org/10.1002/pc.27073
51. Miaudet P, Derré A, Maugey M, Zakri C, Piccione PM, Inoubli R, Poulin P (2007) Shape and Temperature Memory of Nanocomposites with Broadened Glass Transition. Science 318 (5854):1294-1296. doi:doi:10.1126/science.1145593
52. Wang A, Li G, Meng H (2013) Strain rate effect on the thermomechanical behavior of a thermoset shape memory polymer. Smart Mater Struct 22:085033. doi:10.1088/0964-1726/22/8/085033

53. Erdenedelger G, Kim JH, Choi JT, Dao TD, Oh KM, Lee H-i, Jeong HM Shape memory polyurethane nanocomposites with a functionalized graphene. In: Ifost, 2013. IEEE, pp 124-127
54. Liu T, Li J, Pan Y, Zheng Z, Ding X, Peng Y (2011) A new approach to shape memory polymer: design and preparation of poly (methyl methacrylate) composites in the presence of star poly (ethylene glycol). Soft Matter 7 (5):1641-1643
55. Yu K, Ge Q, Qi HJ (2014) Effects of stretch induced softening to the free recovery behavior of shape memory polymer composites. Polymer 55 (23):5938-5947. doi:https://doi.org/10.1016/j.polymer.2014.06.050
56. Liu Y, Han C, Tan H, Du X (2010) Thermal, mechanical and shape memory properties of shape memory epoxy resin. Materials Science and Engineering: A 527 (10):2510-2514. doi:https://doi.org/10.1016/j.msea.2009.12.014
57. Qi X, Yao X, Deng S, Zhou T, Fu Q (2014) Water-induced shape memory effect of graphene oxide reinforced polyvinyl alcohol nanocomposites. Journal of Materials Chemistry A 2 (7):2240-2249
58. Li H, Zhong J, Meng J, Xian G (2013) The reinforcement efficiency of carbon nanotubes/shape memory polymer nanocomposites. Composites Part B: Engineering 44 (1):508-516
59. Du H, Zhang J (2010) Shape memory polymer based on chemically cross-linked poly(vinyl alcohol) containing a small number of water molecules. Colloid and Polymer Science 288 (1):15-24. doi:10.1007/s00396-009-2117-x
60. Kuki Á, Czifrák K, Karger-Kocsis J, Zsuga M, Kéki S (2015) An approach to predict the shape-memory behavior of amorphous polymers from Dynamic Mechanical Analysis (DMA) data. Mechanics of Time-Dependent Materials 19 (1):87-93. doi:10.1007/s11043-014-9253-5
61. Wang Z, Liu J, Guo J, Sun X, Xu L (2017) The Study of Thermal, Mechanical and Shape Memory Properties of Chopped Carbon Fiber-Reinforced TPI Shape Memory Polymer Composites. Polymers 9 (11):594
62. Ahmed N, Niaz B, Ahmed S, Javid MT, Ali M, Tariq M (2023) Mechanically robust and highly elastic thermally induced shape memory polyurethane based composites for smart and sustainable robotic applications. Polymers for Advanced Technologies 34 (4):1182-1196. doi:https://doi.org/10.1002/pat.5961
63. Liu Y, Li Y, Yang G, Zheng X, Zhou S (2015) Multi-Stimulus-Responsive Shape-Memory Polymer Nanocomposite Network Cross-Linked by Cellulose Nanocrystals. ACS Applied Materials & Interfaces 7 (7):4118-4126. doi:10.1021/am5081056
64. Zhai W, Srikanth N, Kong LB, Zhou K (2017) Carbon nanomaterials in tribology. Carbon 119:150-171
65. Goh PS, Ismail AF, Ng BC (2014) Directional alignment of carbon nanotubes in polymer matrices: Contemporary approaches and future advances. Composites Part A: Applied Science and Manufacturing 56:103-126. doi:https://doi.org/10.1016/j.compositesa.2013.10.001
66. Chen K, Li M, Yang Z, Ye Z, Zhang D, Zhao B, Xia Z, Wang Q, Kong X, Shang Y, Liu C, Yu H, Cao A (2024) Ultra-Large Stress and Strain Polymer Nanocomposite Actuators Incorporating a Mutually-Interpenetrated, Collective-Deformation Carbon Nanotube Network. Advanced Materials n/a (n/a):2313354. doi:https://doi.org/10.1002/adma.202313354
67. Tcharkhtchi A, Abdallah-Elhirtsi S, Ebrahimi K, Fitoussi J, Shirinbayan M, Farzaneh S (2014) Some New Concepts of Shape Memory Effect of Polymers. Polymers 6 (4):1144-1163
68. Nunes MABS, de Matos BR, Silva GG, Ito EN, de Melo TJA, Fechine GJM (2021) Hybrids nanocomposites based on a polymer blend (linear low-density polyethylene/poly(ethylene-co-methyl acrylate) and carbonaceous fillers (graphene and carbon nanotube). Polym Compos 42 (2):661-677. doi:https://doi.org/10.1002/pc.25856
69. Raj R, Maroo SC, Wang EN (2013) Wettability of Graphene. Nano Lett 13 (4):1509-1515. doi:10.1021/nl304647t
70. Su K-H, Su C-Y, Cho C-T, Lin C-H, Jhou G-F, Chang C-C (2019) Development of Thermally Conductive Polyurethane Composite by Low Filler Loading of Spherical BN/PMMA Composite Powder. Scientific Reports 9 (1):14397. doi:10.1038/s41598-019-50985-5

71. Gao J, Hu M, Dong Y, Li RKY (2013) Graphite-Nanoplatelet-Decorated Polymer Nanofiber with Improved Thermal, Electrical, and Mechanical Properties. ACS Applied Materials & Interfaces 5 (16):7758-7764. doi:10.1021/am401420k
72. Hatui G, Bhattacharya P, Sahoo S, Dhibar S, Das CK (2014) Combined effect of expanded graphite and multiwall carbon nanotubes on the thermo mechanical, morphological as well as electrical conductivity of in situ bulk polymerized polystyrene composites. Composites Part A: Applied Science and Manufacturing 56:181-191. doi:https://doi.org/10.1016/j.compositesa.2013.10.007
73. Xu Q, Zhai H, Wang G (2015) Mechanism of smoke suppression by melamine in rigid polyurethane foam. Fire and Materials 39 (3):271-282. doi:https://doi.org/10.1002/fam.2249
74. Dwivedi N, Neogi A, Patra TK, Dhand C, Dutta T, Yeo RJ, Kumar R, Hashmi SAR, Srivastava AK, Tripathy S, Saifullah MSM, Sankaranarayanan SKRS, Bhatia CS (2021) Angstrom-Scale Transparent Overcoats: Interfacial Nitrogen-Driven Atomic Intermingling Promotes Lubricity and Surface Protection of Ultrathin Carbon. Nano Letters 21 (21):8960-8969. doi:10.1021/acs.nanolett.1c01997